WAVE ENERGY EXTRACTION FROM AN OSCILLATING WATER COLUMN IN A TRUNCATED CIRCULAR CYLINDER

A Thesis

by

HAO WANG

Submitted to the Office of Graduate Studies of
Texas A&M University
in partial fulfillment of the requirements for the degree of

MASTER OF SCIENCE

Chair of Committee,	Jeffrey Falzarano
Committee Members,	Alan Palazzolo
	Moo-Hyun Kim
Head of Department,	Robin Autenrieth

August 2013

Major Subject: Ocean Engineering

ABSTRACT

Oscillating Water Column (OWC) device is a relatively practical and convenient way that converts wave energy to a utilizable form, which is usually electricity. The OWC is kept inside a fixed truncated vertical cylinder, which is a hollow structure with one submerged open end in the water and with an air turbine at the top. The research adopts potential theory and Galerkin methods to solve the motion of the OWC. Based on the air-water interaction model, optimal OWC design for energy extraction from regular wave is explored.

The hydrodynamic coefficients in scattering and radiation potential are solved using Galerkin approximation. The numerical results for the free surface elevation have been verified by a series of experiments conducted in the University of New Orleans Towing Tank. The effect of geometric parameters on the response amplitude operator (RAO) of OWC is studied and amendment of the equation for evaluating the natural frequency of the OWC is made.

Using the model of air-water interaction under certain wave parameters and OWC geometric parameters, a computer program OWC Solution is developed to optimize the energy output from the system. Optimization results by the program OWC Solution lead to an effective method to design the OWC system.

TABLE OF CONTENTS

Page

Page

LIST OF FIGURES

Page

Page

LIST OF TABLES

Page

Page

Page

1. INTRODUCTION

For a half century, the increasing demand for energy has been driving scientists and engineers into finding new energy resources. Wave energy is viewed as a promising renewable energy resource and more than 150 wave energy extraction device concepts have been created, including attenuator, point absorber, overtopping device and other new technologies (Falzarano et al., 2012).

Among the wave energy conversion devices, the Oscillating Water Column (OWC) device is a fixed cylinder with air flow output from it driven by the wave elevation inside the device. Usually an air turbine is installed with a system to convert the motion of the air flow into electricity. Garrett (1970) first studied the progressive wave induced fluid motion inside a hollow cylinder partially immerged in finite water depth. Sarmento and Falcão (1985) did a two-dimensional analysis for an OWC device using linear wave theory. Malmo & Reitan (1985) conducted calculations of the wave power absorption by a squared oscillating water column in a channel. Linton and Evans (1992) studied the wave scattering and radiation by a vertical circular cylinder placed on a channel using the multipole method. Evans and Porter (1995, 1997) came up with a powerful and accurate numerical method to solve for the OWC hydrodynamic coefficients using Galerkin method with accuracy and efficiency. Falnes (2002) developed a theoretical model for the OWC device with a pneumatic power takeoff. Cho (2002) studied the energy output from an OWC in a circular cylinder for a real-valued

turbine constant. Garriga and Falzarano (2008) calculated the water surface elevation using existing potential theory and compared it with the experiments result from the UNO towing tank. Koo and Kim (2010, 2012) conducted a time-domain simulation of a 2-D land-based Oscillating Water Column using nonlinear model with viscous damping, and they got a good comparison with experimental results. Alves et al. (2011) made implementation to a time-domain model to analyze the dynamics of a WEC (Wave Energy Converter) and verified the numerical simulation codes like WAMIT. Using either numerical or experimental method, scholars such as Gato and Falcão (1984, 1988), Kaneko, Setoguchi, and Inoue (1986) and Camporeale, Filianoti and Torresi (2011) conducted research on Wells turbine, which is widely used for OWC device.

The purpose of this thesis is to combine the existing potential theory for the scattering and the radiation problem for a truncated vertical cylinder with the model for the interaction between water surfaces and air flow through a turbine and to make a complete program to solve and optimize OWC device design. In this research, the numerical method from Evans and Porter is verified again and extensive results about the energy output from the system are given. This thesis also discusses the limitation for OWC optimization and tries to explore the effect of the aerodynamic characteristics of the air turbine on the OWC system energy output.

In order to show a complete theoretical background of the numerical model, the author follows the derivation procedure by Evans and Porter (1997).

2. MATHEMATICAL MODEL

2.1 Governing Equations

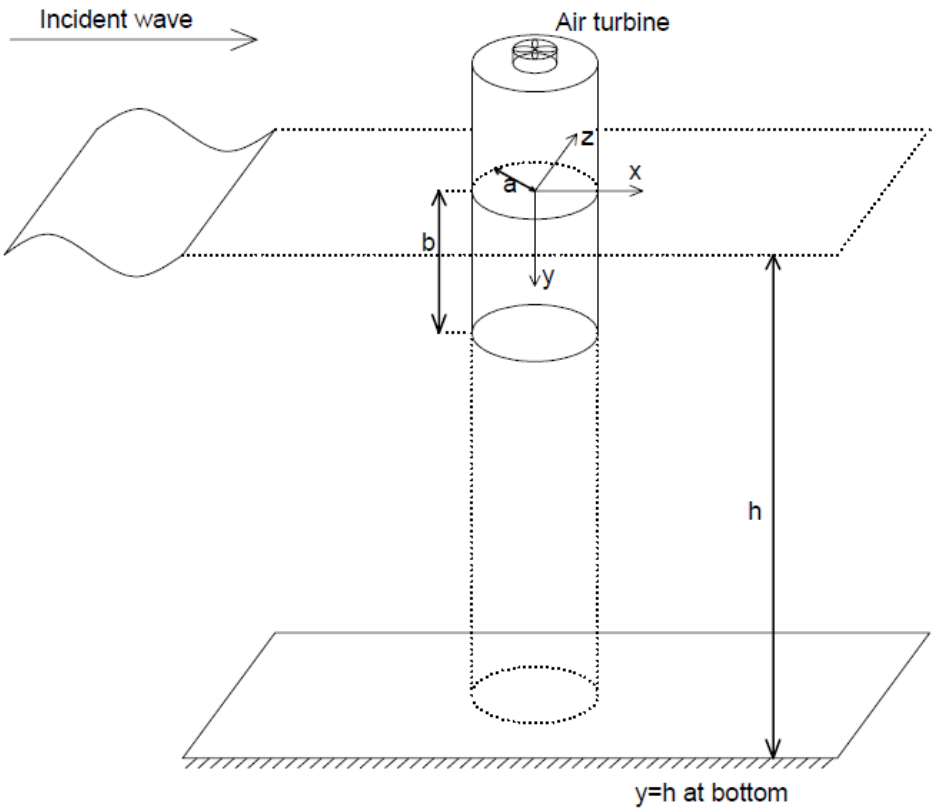

Figure 1. Concept of the OWC device

This subsection follows the work by Evans and Porter (1995) and Garriga (2003) to show the mathematical foundation of an OWC device. Figure 1 shows the basic concept of the OWC device.

Base on the Laplace equation:

$$\nabla^2\Phi(x,y,z,t) = 0, \nabla^2 = (\frac{\partial^2}{\partial x^2}, \frac{\partial^2}{\partial y^2}, \frac{\partial^2}{\partial z^2})^T$$

$\Phi(x,y,z,t)$ represents the velocity potential. On fixed boundary:

$$\frac{\partial \Phi}{\partial \tilde{n}} = 0$$

$\tilde{n}$ is the normal vector to fixed boundary. The Linearized Kinematic Free Surface Boundary Condition is:

$$\frac{\partial \eta}{\partial t} = \frac{\partial \Phi}{\partial y}|_{y=0}$$

Here η is the surface elevation measured downwards. Inside the cylinder, the Linearized Dynamic Free Surface Boundary Condition is:

$$\frac{\partial \Phi}{\partial t}|_{y=0} + \frac{P(t)}{\rho} - g\eta = 0$$

Outside the cylinder, the Linearized Dynamic Free Surface Boundary Condition is:

$$\frac{\partial \Phi}{\partial t}|_{y=0} - g\eta = 0$$

$P(t)$ is the time dependent fluctuating air pressure inside the cylinder.

2.2 Solution of the Wave Potential

The following subsection follows Evans and Porter's (1997) and Garriga and Falzarano's (2008) derivation to solve the wave potential.

Take the time derivative to LDFSBC. Inside the cylinder:

$$\frac{\partial \eta}{\partial t} = \frac{1}{g}\frac{\partial^2 \Phi}{\partial t^2}|_{y=0} + \frac{1}{\rho g}\frac{\partial P(t)}{\partial t}$$

Outside the cylinder:

$$\frac{\partial \eta}{\partial t} = \frac{1}{g}\frac{\partial^2 \Phi}{\partial t^2}|_{y=0}$$

We assume a harmonic wave with time dependence $e^{-i\omega t}$.ω is the angular frequency of the incident wave. The pressure oscillation and wave elevation have the same frequency because of linearity, so:

$$\Phi(x,y,z) = Re\{\phi(x,y,z)e^{-i\omega t}\}$$

$$\eta(x,z,t) = Re\{\eta(x,z)e^{-i\omega t}\}$$

$$p_e = Re\{pe^{-i\omega t}\}$$

p_e is the oscillating part of the air pressure. ($P(t) = p_a + p_e$,p_a is the atmosphere air pressure). We can remove the time dependence of the fluid potential to deal with the time-independent potential, denoted by ϕ. Apply Laplace equation:

$$\nabla^2 \phi = 0$$

Apply the LDFSBC, inside the cylinder:

$$g\eta + i\omega\phi = \frac{p}{\rho}$$

Outside the cylinder:

$$g\eta + i\omega\phi = 0$$

Combine the KFSBC and LDFSBC. Inside the cylinder:

$$\frac{\partial \phi}{\partial y}|_{(y=0)} + \frac{\omega^2}{g}\phi|_{(y=0)} = -\frac{i\omega}{\rho g}p$$

Outside the cylinder:

$$\frac{\partial \phi}{\partial y}|_{y=0} + \frac{\omega^2}{g}\phi|_{y=0} = 0$$

According to Evans (1982), the time-independent potential can be decomposed into two parts:

$$\phi = \phi^S - \frac{i\omega p}{\rho g}\phi^R$$

In which ϕ^S is the scattering potential (related to the incident and diffraction waves under constant air pressure on the water surface inside the cylinder).ϕ^R is the radiation potential related to the radiated waves due to oscillating air pressure on the water surface inside the cylinder. According to Evans and Porter (1997), apply the radiation potential to the LCFSBC. Inside the cylinder:

$$\frac{\partial \phi^R}{\partial y}|_{y=0} + \frac{\omega^2}{g}\phi^R|_{y=0} = 1$$

Outside the cylinder:

$$\frac{\partial \phi^R}{\partial y}|_{y=0} + \frac{\omega^2}{g}\phi^R|_{y=0} = 0$$

Since the scattering potential is separated from the air pressure related term, the LCFSBC for scattering potential is:

$$\frac{\partial \phi^S}{\partial y}|_{y=0} + \frac{\omega^2}{g}\phi^S|_{y=0} = 0$$

It is more convenient to express the wave potential in cylindrical coordinate system(r, θ, y).The Laplace equation in cylindrical coordinates is:

$$\frac{1}{r}\frac{\partial}{\partial r}\left(r\frac{\partial \phi}{\partial r}\right) + \frac{1}{r^2}\frac{\partial^2 \phi}{\partial \theta^2} + \frac{\partial^2 \phi}{\partial y^2} = 0$$

At the bottom, the vertical velocity must be zero. (The water depth is denoted by h.)

$$\frac{\partial \phi}{\partial y}|_{y=h} = 0$$

The body surface boundary condition is:

$$\frac{\partial \phi}{\partial r} = 0, \ \ for\ 0 < y < b\ and\ r = a$$

The potential can be solved using separation of variable:

$$\phi(r, \theta, y) = \varphi_i(r, \theta)\psi_i(y)$$

By separation of variables, we can achieve the general form of solution to the Laplace equation as an eigenfunctions expansion:

$$\frac{1}{\varphi_i}\frac{1}{r}\frac{\partial}{\partial r}\left(r\frac{\partial \varphi_i}{\partial r}\right) + \frac{1}{\varphi_i}\frac{1}{r^2}\frac{\partial^2 \varphi_i}{\partial \theta^2} = {k_i}^2$$

$$\frac{1}{\psi_i}\frac{\partial^2 \psi_i}{\partial y^2} = -{k_i}^2$$

The boundary condition for ψ_i is:

$$\frac{\partial \psi_i}{\partial y}|_{y=h} = 0$$

$$\frac{\partial \psi_i}{\partial y}|_{y=0} + \frac{\omega^2}{g}\psi_i|_{y=0} = 0$$

The rest part in this subsection is given according to solutions of partial differential equation by Haberman (2004).

According to typical solution to ordinary differential equation:

$$\psi_i = a_1 cos[k_i(h - y)] + a_2 sin[k_i(h - y)]$$

And:

$$\frac{\partial \psi_i}{\partial y}|_{y=h} = -a_2 k_i = 0$$

When k_i=0, all solutions will be trivial. So a_2=0.

$$\psi_i = a_1 cos[k_i(h-y)]$$

Apply the linearized free surface boundary condition:

$$\frac{\partial \psi_i}{\partial y}|_{y=0} + \frac{\omega^2}{g}\psi_i|_{y=0} = k_i A sin(k_i h) + A\frac{\omega^2}{g}cos(k_i h) = 0$$

So k_i satisfies:

$$\frac{\omega^2}{g} + k_i\, tan(k_i h) = 0$$

The equation can also have imaginary solution. When $k_0 = ik$, k is the wave number for progressive wave.

$$\psi_0 = a_1 cosh[k(h-y)]$$

According to:

$$cosh(x) = cos(ix), tan\, h(x) = -i \cdot tan(ix)$$

The progressive wave dispersion relationship is:

$$\frac{\omega^2}{g} = k\, tanh(kh)$$

We can use the orthogonal identity of the eigenfunction to solve for a_1. If we write $\varphi_i(r,\theta) = f(r)g(\theta)$, we get:

$$\frac{1}{f}\frac{1}{r}\frac{\partial}{\partial r}\left(r\frac{\partial f}{\partial r}\right) + \frac{1}{g}\frac{1}{r^2}\frac{\partial^2 g}{\partial \theta^2} = {k_i}^2$$

Multiply both sides with $r^2$and separate the two eigenfunctions:

$$-\frac{1}{g}\frac{d^2g}{d\theta^2} = \mu$$

$$r\frac{\partial}{\partial r}\left(r\frac{\partial f}{\partial r}\right) + \left(-{k_i}^2 r^2 - \mu\right)f = 0$$

According to the symmetry of the flow around the cylinder, at $\theta = 0$, the tangential velocity must be zero:

$$\frac{dg}{d\theta}(0) = 0$$

According to the solution to ordinary differential equation:

$$g(\theta) = b_1\cos(q\theta) + b_2\sin(q\theta)$$

So $b_2 = 0$.

$$g(\theta) = b_1\cos(q\theta)$$

When $-{k_i}^2 > 0$, only one wave number $k_0 = k$ suitable for the solution. So:

$$f(r) = c_1 H_q^{(1)}(kr) + c_2 H_q^{(2)}(kr), \qquad where\ \mu = q^2$$

When ${k_i}^2 > 0$, there are wave numbers k_i for the solution. This is the standing waves eigenfunction in radial coordinates:

$$f(r) = c_3 I_q(k_i r) + c_4 K_q(k_i r), \qquad where\ \mu = q^2$$

This section gives the general form of eigenfunction expansion for the wave potential. In the following section when we are solving the scattering and radiation problem, we will adopt the form above.

3. THE SCATTERING PROBLEM

3.1 The Solution for the Hydrodynamic Coefficients in Scattering Problem

Scattering problem is induced by the incident wave when there is no radiation. For progressive wave that travels in positive x direction, the time-independent incident wave potential can be written as:

$$\phi^I = e^{ikx}\psi_0(y)$$

Chakrabarti (1987) gives the following equation:

$$e^{ikx} = \sum_{q=0}^{\infty} \epsilon_q \, i^q J_q(kr)\cos(q\theta)$$

$$where\ \epsilon_0 = 1, \epsilon_q = 2, for\ q \geq 1$$

The derivation in this subsection was given according to Evans and Porter (1997).

The scattering potential in a cylindrical coordinate system is ϕ^S.Outside the cylinder ($r \geq a$):

$$\phi^S = \sum_{q=0}^{\infty} \epsilon_q \, i^q \, cos(q\theta) \left[\left(J_q(kr) + \alpha_{q,0}^S H_q(kr) \right) \psi_0(y) + \sum_{i=1}^{\infty} \alpha_{q,i}^S \, K_q(k_i r)\psi_i(y) \right]$$

The first term represents the incident waves; the second term associated with $\alpha_{q,0}^S H_q(kr)$ is the outgoing progressive waves, and the last term with $\alpha_{q,i}^S K_q(k_i r)$ is the wave modes which are exponentially decaying.

Inside the cylinder ($r \leq a$):

$$\phi^S = \sum_{q=0}^{\infty} \epsilon_q \, i^q \cos(q\theta) \left[\beta_{q,0}^S J_q(kr)\psi_0(y) + \sum_{i=1}^{\infty} \beta_{q,i}^S \, I_q(k_i r)\psi_i(y) \right]$$

The first term associated with $\beta_{q,0}^{S}$ is the standing wave modes inside the cylinder, and the $\beta_{q,n}^{S}$ terms are the exponentially decaying disturbances. $\psi_0(y)$ and $\psi_i(y)$ are the eigenfunctions in the y direction, if we write:

$$\psi_0(y) = \frac{1}{M_0}\cosh k(h-y), \quad i = 0$$

$$\psi_i(y) = \frac{1}{M_i}\cos k_i(h-y), \quad i \geq 1$$

Then:

$$M_0 = \sqrt{\frac{1}{2}\left(1 + \frac{sinh2kh}{2kh}\right)}$$

$$M_i = \sqrt{\frac{1}{2}(1 + \frac{sin2k_ih}{2k_ih})}$$

$k\ and\ k_i$ are the wave numbers which satisfy the dispersion relation given in the previous section. We can calculate the progressive wave number from the dispersion relationship. k can also be written as k_p. When the incident wave frequency ω=1.5rad/s, and the water depth h=20ft, the dispersion relationship is shown in Figure 2:

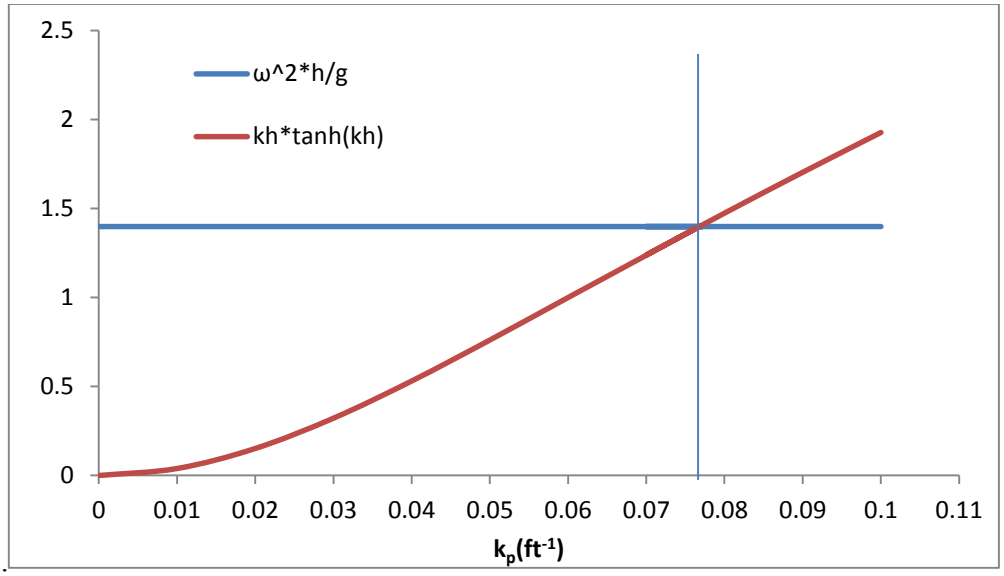

Figure 2. Progressive wave number

The computer program OWC Solution gives k_p =0.077 ft^{-1}, corresponding to the wavelength of 81.87ft. The standing wave modes are given in Figure 3:

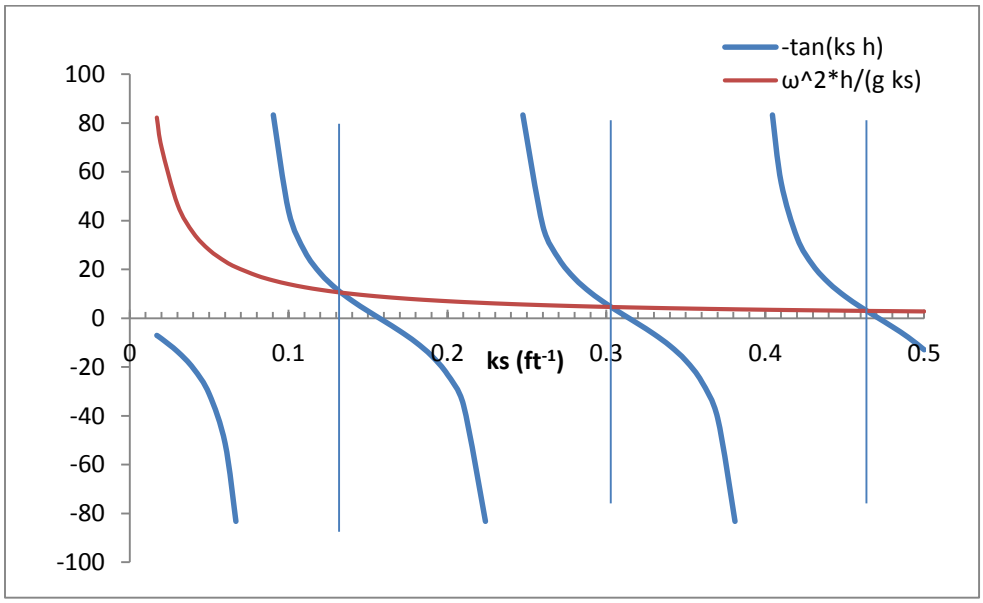

Figure 3. Standing wave numbers

Using the computer program OWC Solution, we can calculate the first 100 standing wave numbers. Here are the first three wave modes for comparison:

k_1 =0.133 ft^{-1}; k_2 =0.303 ft^{-1}; k_3 =0.464 ft^{-1}; which match Figure 3.

Evans and Porter (1997) derived the following transformation of boundary conditions before using the Galerkin approximation. If we rewrite the scattering potential as:

$$\phi^S = \sum_{q=0}^{\infty} \epsilon_q \, i^q \cos(q\theta) \, \Psi_q^S(r, y)$$

We can define $U_q^S(y)$ as:

$$U_q^S(y) = \frac{\partial \Psi_q^S}{\partial r}|_{r=a}$$

Based on the continuity of radial velocity, the radial velocity at the radius of the cylinder should be consistent whether we calculate it according to the potential expression outside the cylinder or expression inside the cylinder. After removing the y-direction eigenfunctions, we can achieve the relation between the hydrodynamic coefficients of the potential:

$$kJ_q'(ka) + \alpha_{q,0}^S kH_q'(ka) = \beta_{q,0}^S kJ_q'(ka) = \frac{1}{h}\int_b^h U_q^S(y)\psi_0(y)dy$$

$$\alpha_{q,i}^S k_i K_q'(k_i a) = \beta_{q,i}^S k_i I_q'(k_i a) = \frac{1}{h}\int_b^h U_q^S(y)\psi_i(y)dy$$

Since both inside and outside of the cylinder belong to the same fluid domain, the velocity potential should be continuous at the radius of the cylinder. So we can achieve another equation between the coefficients of potential inside and outside the cylinder:

$$0 = \left(J_q(ka) + \alpha_{q,0}^S H_q(ka) - \beta_{q,0}^S J_q(ka)\right)\psi_0(y) + \sum_{i=1}^{\infty}(\alpha_{q,i}^S K_q(k_i a) - \beta_{q,i}^S I_q(k_i a))\psi_i(y)$$

Using the Wronskian identity for Bessel functions, we can combine the two boundary conditions. Evans and Porter (1997) got:

$$\int_b^h U_q^S(t) L_q(y,t)dt = \frac{-2i\alpha_{q,0}^S}{\pi ka J_q'(ka)}\psi_0(y)$$

In which:

$$L_q(y,t) = -\sum_{i=1}^{\infty}\frac{\psi_i(y)\psi_i(t)}{k_i^2 ha I_q'(k_i a)K_q'(k_i a)}$$

Evans and Porter (1997) set:

$$U_0^S(y) = \frac{2i\alpha_{0,0}^S}{\pi ka J_1(ka)}u_2(y)$$

$$\int_b^h u_2(t) L_0(y,t)dt = \psi_0(y)$$

For higher order q:

$$U_q^S(y) = \frac{-2i\alpha_{q,0}^S}{\pi ka J_q'(ka)}u_q^S(y)$$

$$\int_b^h u_q^S(l) L_q(y,l)dt = \psi_0(y)$$

The scattering induced volume flux across the free surface is:

$$q^S = -\int_d^h \int_0^{2\pi} \frac{\partial \phi^S}{\partial r}\Big|_{r=a} a d\theta dy = \frac{-4ia\alpha_{0,0}^S}{ka J_1(ka)}\int_a^h u_2(y)\cdot 1 dy$$

3.2 The Galerkin Approximation

The equations in the following subsection were derived by Evans and Porter (1997), and they are used as the numerical foundation of my computer program.

If:

$$\int_b^h u_i(l)L_0(y,l)dt = e_i(y)\ , where\ e_1 = 1, e_2 = \psi_0$$

Then:

$$\int_b^h u_i\ e_j dy = S_{ij}\ , where\ e_1 = 1, e_2 = \psi_0$$

{S} can be calculated from:

$$S \cong D^T L^{(0)^{-1}} D$$

In which $L^{(0)}$ is a $(N+1) \times (N+1)$ matrix, and D is a $(N+1) \times 2$ matrix:

$$L_{mn}^{(0)} = \sum_{r=1}^{\infty} \frac{J_{2m}\{k_r(h-b)\}J_{2n}\{k_r(h-b)\}}{M_r^2 k_r h k_r a I_1(k_r a)K_1(k_r a)}$$

$$D_{1m} = \delta_{m0}\ , D_{2m} = (-1)^m \frac{1}{M_0} I_{2m}\{k(h-b)\}$$

And if we have:

$$\int_b^h u_q^S\ (l)L_q(y,l)dt = \psi_0(y)$$

Then:

$$A_q^S = \int_b^h u_q^S \cdot \psi_0 dy \cong F^T L^{(q)^{-1}} F$$

Where $F = (F_0, \dots, F_N)^T$;

$$F_m = (-1)^m \frac{1}{M_0} I_{2m}\{k(h-b)\}$$

And:

$$L_{mn}^{(q)} = -\sum_{r=1}^{\infty} \frac{J_{2m}\{k_r(h-b)\}J_{2n}\{k_r(h-b)\}}{M_r^2 k_r h k_r a I_q'(k_r a) K_q'(k_r a)}$$

This is the numerical method for us to calculate the hydrodynamic coefficients. According to Galerkin approximation above, Evans and Porter (1997) got:

$$\alpha_{0,0}^S = \frac{-\pi kakhJ_1^2(ka)}{\pi kakhJ_1(ka)H_1(ka) + 2iS_{22}}$$

$$\alpha_{q,0}^S = \frac{-\pi kakhJ_q'(ka)J_q'(ka)}{\pi kakhJ_q'(ka)H_q'(ka) + 2iA_q^S}$$

$$q^S = \frac{4\pi ikahJ_1(ka)S_{21}}{\pi kakhJ_1(ka)H_1(ka) + 2iS_{22}}$$

3.3 Discussion of Convergence of Evans Model

Table 1 is a sample solution to hydrodynamic coefficients. The incident wave frequency ω=1.2 rad/s; the radius a=4 ft; the draft b= 10 ft; the water depth h=30 ft.

Table 1: Hydrodynamic coefficients solution

q	Re($\alpha_{q,0}^S$)	Im($\alpha_{q,0}^S$)	Re($\beta_{q,0}^S$)	Im($\beta_{q,0}^S$)
0	-2.315E-05	4.811E-03	1.163E+00	5.597E-03
1	-2.178E-04	1.476E-02	5.263E-01	7.767E-03
2	-6.260E-09	7.912E-05	4.755E-01	3.762E-05
3	-1.776E-14	1.333E-07	4.611E-01	6.145E-08
4	-1.224E-20	1.106E-10	4.544E-01	5.028E-11
5	-3.005E-27	5.482E-14	4.506E-01	2.470E-14
6	-3.261E-34	1.806E-17	4.480E-01	8.090E-18
7	-1.800E-41	4.242E-21	4.462E-01	1.893E-21
8	-5.576E-49	7.467E-25	4.449E-01	3.322E-25

We can observe that the hydrodynamic coefficients (except for the real part of $\beta_{q,0}^{S}$) are decaying quickly with respect to the order q, which is typical for these calculations. We should also notice that the Bessel function is also decaying with respect to its order q. Table 2 is the decaying series of Bessel functions with respect to order q. (the wave number k=0.05 ft^{-1}, and r = 4 ft.)

Table 2: Bessel function values

q	$J_q(kr)$	q	$J_q(kr)$
0	9.900E-01	5	8.319E-08
1	9.950E-02	6	1.387E-09
2	4.983E-03	7	1.982E-11
3	1.663E-04	8	2.477E-13
4	4.158E-06	kr	0.2

So the fluid potential converges quickly with respect to order q, so we can reach a convergent result with a low order of q (up to 8 in the computer program OWC Solution).

3.4 The Free Surface Elevation Comparison with Experimental Results

The free surface elevation can be used to verify the accuracy of the numerical model. A previous experiment about the water surface elevation was conducted in University of New Orleans by Garriga and Falzarano (2008). The free surface elevation in the experiment is measured at the center of the cylinder (r=0). Using the computer program OWC Solution, we can calculate the water surface elevation at the center of the cylinder and compare it with the experiment results.

If we define the incident wave height as H_{inc}, then the incident wave potential in cylindrical coordinates is:

$$\Phi_{inc} = Re\{\sum_{q=0}^{\infty} \epsilon_q \, i^q J_q(kr)\cos(q\theta)\psi_0(y)\, e^{-i\omega t}\} \cdot \frac{H_{inc}}{2} \cdot \frac{g}{w} \cdot \frac{1}{\psi_0(y)\,|_{y=0}} i$$

The corresponding free surface elevation can be calculated by:

$$\eta_{inc} = \frac{1}{g} \cdot \frac{\partial \Phi_{inc}}{\partial t}|_{y=0}$$

So the incident wave elevation is:

$$\eta_{inc} = Re\{\sum_{q=0}^{\infty} \epsilon_q \, i^q J_q(kr)\cos(q\theta)\, e^{-i\omega t}\} \cdot \frac{H_{inc}}{2}$$

Since we are using linear wave theory, according to the derivations in subsection 3.1, when we multiply the incident wave potential $\phi^I e^{-iwt}$ with $\frac{H_{inc}}{2} \cdot \frac{g}{w} \cdot \frac{1}{\psi_0(y)\,|_{y=0}} i$, we will get the wave potential when the incident wave height is H_{inc}.

So the wave potential inside the cylinder is:

$$\Phi_{OWC} = Re\{\phi^S \cdot e^{-iwt} \cdot \frac{H_{inc}}{2} \cdot \frac{g}{w} \cdot \frac{1}{\psi_0(y)\,|_{y=0}} i\}$$

Similarly, the free surface elevation inside the cylinder is:

$$\eta_{OWC} = \frac{1}{g} \cdot \frac{\partial \Phi_{OWC}}{\partial t}|_{(y=0)}$$

If we define the wave height at the center of the cylinder as H_{OWC}:

$$H_{OWC} = Re\{\sum_{q=0}^{\infty} \epsilon_q \, i^q \cos(q\theta)\left[\beta_{q,0}^S J_q(kr)\psi_0(y) + \sum_{i=1}^{\infty} \beta_{q,i}^S \, I_q(k_i r)\psi_i(y)\right] e^{-i\omega t}\} \cdot \frac{H_{inc}}{2}$$

At the center of the cylinder: $r = 0, \theta = 0, y = 0$:(Experimental measurements were made at this coordinate.)

$$\frac{H_{OWC}}{H_{inc}} = \frac{|\sum_{q=0}^{\infty} \epsilon_q \, i^q \, cos(q\theta) \left[\beta_{q,0}^{S} J_q(kr)\psi_0(y) + \sum_{i=1}^{\infty} \beta_{q,i}^{S} \, I_q(k_i r)\psi_i(y)\right]|}{|\sum_{q=0}^{\infty} \epsilon_q \, i^q J_q(kr) \, cos(q\theta)\,|}$$

H_{OWC} and H_{inc} are defined as a real number with a phase of θ_η and θ_0 respectively. The Visual Basic program OWC Solution can solve for the hydrodynamic coefficients $\beta_{q,0}^{S}$ corresponding to the qth order of the expansion, and then we can calculate the wave height at any point inside the cylinder. Furthermore, the solution to the wave potential in the fluid field can give you the fluid velocity and the fluid pressure (first order) at any point, so extensive experimental verification can be done.

Table 3 shows the parameters used by Garriga and Falzarano (2008) in the UNO model test. Table 4 shows the experimental result given by Garriga and Falzarano (2008) for the draft b=2.5 ft. Figure 4 is the plot of the comparison between experimental and numerical result when b=2.5 ft.

Table 3: Experiment and numerical calculation parameters (Case 1)

Parameter	Radius(ft.)	Draft(ft.)	Water Depth(ft.)
-	1	2.5	6.33
Minimum ω	$\omega^2 h/g$	Maximum ω	$\omega^2 h/g$
1.5	0.442	8.212	13.26

Table 4: Experiment data for b=2.5 ft

ω	$\omega^2 h/g$	H_{OWC}/H_{inc}
8.4380	14.00	0.00
6.3785	8.00	0.05
4.9665	4.85	0.10
4.5103	4.00	0.16
4.1583	3.40	0.55
3.6363	2.60	1.70
3.2524	2.08	2.65
3.1893	2.00	2.55
2.8526	1.60	1.67
1.9530	0.75	1.30

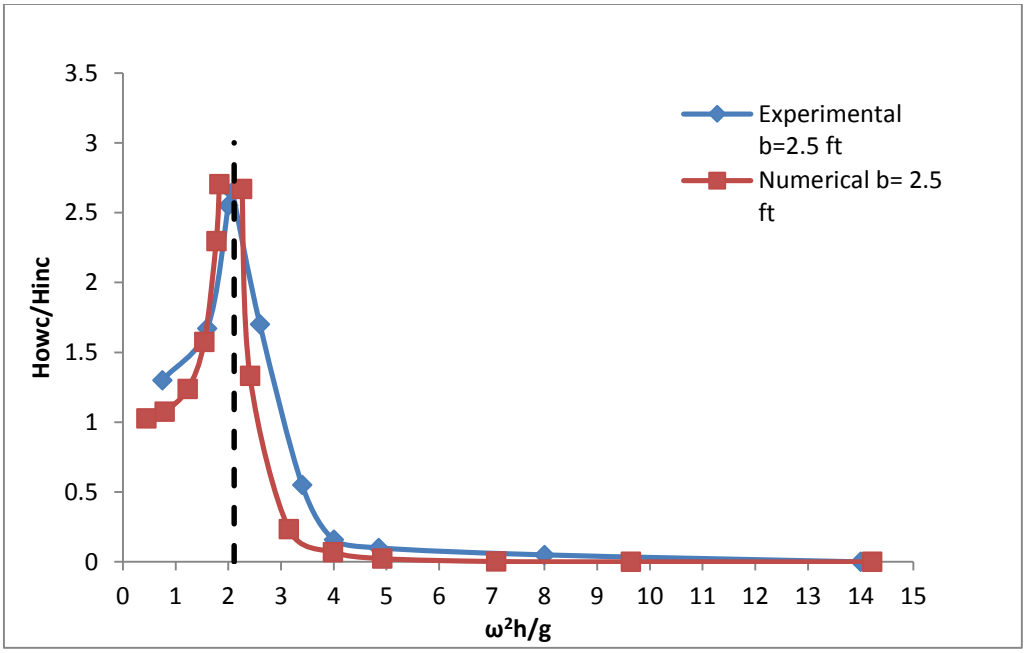

Figure 4. Comparison between experimental and numerical result (b=2.5 ft)

Table 5 shows the parameters used by Garriga and Falzarano (2008) in the UNO model test. Table 6 shows the experimental result given by Garriga and Falzarano (2008)

for the draft b=1.67 ft. Figure 5 is the plot of the comparison between experimental and numerical result when b=1.67 ft.

Table 5: Experiment and numerical calculation parameters (Case 2)

Parameter	Radius(ft.)	Draft(ft.)	Water Depth(ft.)
-	1	1.67	6.33
Minimum ω	$\omega^2 h/g$	Maximum ω	$\omega^2 h/g$
1.953	0.75	8.438	14

Table 6: Experiment data for b=1.67 ft

ω	$\omega^2 h/g$	H_{OWC}/H_{inc}
8.436	14.00	0.00
5.041	5.00	0.40
4.509	4.00	0.95
4.188	3.45	1.75
3.905	3.00	2.50
3.806	2.85	2.45
3.739	2.75	2.26
3.565	2.50	2.00
2.761	1.50	1.35
2.054	0.83	1.16

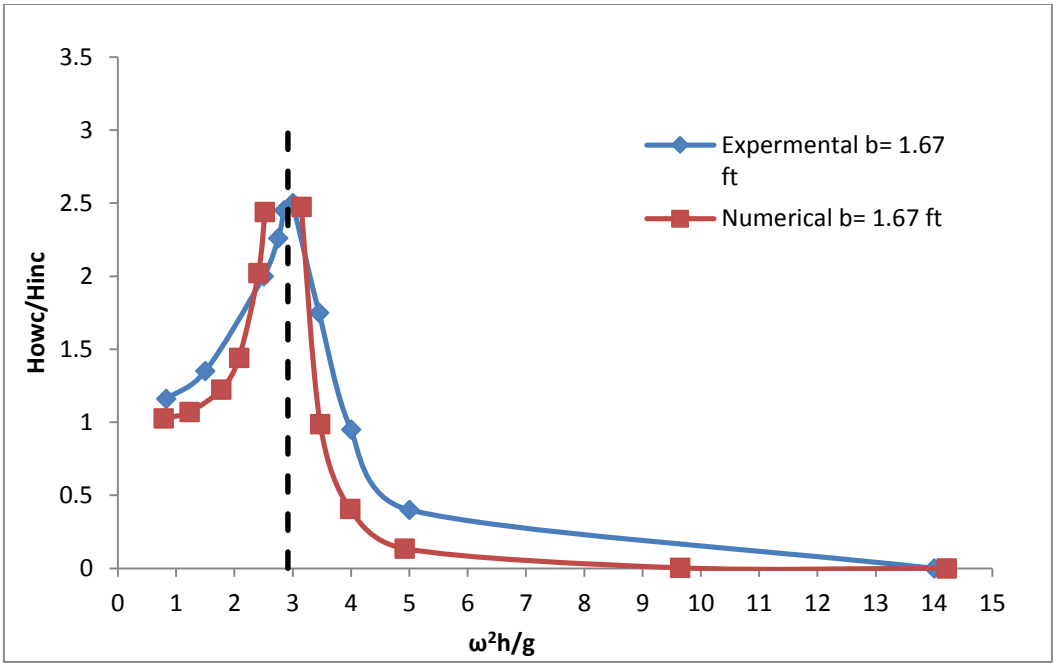

Figure 5. Comparison between experimental and numerical result (b=1.67 ft)

3.5 The Natural Frequency Approximation

Faltinsen (1990) gave the natural frequency equation of a moon pool: $\omega_n = \sqrt{\frac{g}{b}}$, which is an approximation of the heave natural frequency of a floating walled body without the added mass effect.

According to Karami, Ketabdari, and Akhtari (2012), we can generally write the equation of motion for the oscillating water column as:

$$(m + m_a)\frac{d^2\eta}{dt^2} + (B_r + B_a)\frac{d\eta}{dt} + K_r\eta = F_S$$

m is the mass of water column inside the cylinder at its equilibrium, m_a is the added mass of water column, B_r is the radiation damping coefficient, B_a is the applied

damping coefficients, K_r is hydrostatic stiffness, and F_S is the exciting force due to the scattering (incident and diffraction) potential. The viscous damping is not considered in this model.

According to the added mass of the oscillating water column by Falnes (2002), an amendment to Faltinsen's (1990) approximation for the natural frequency is given to estimate the natural frequency:

$$\omega_n = \sqrt{\frac{\rho g \pi a^2}{\rho \pi a^2 b + 0.5\pi\rho a^3}} = \sqrt{\frac{g}{b + 0.5a}}$$

In which $\rho g \pi a^2$ represents the hydrostatic stiffness of the OWC system because the restoring force is the resultant force of gravity and buoyancy. $F_R = -\rho g \pi a^2 \eta$, η is the internal wave elevation. When η is positive, the gravity of the elevated water column will be the restoring force, and when η is negative, the additional buoyance of the submerged water column will be the restoring force.

$\rho \pi a^2 b$ is the mass of water column inside the cylinder at its equilibrium position in vertical direction; $0.5\pi\rho a^3$ is the approximation for added mass of the water column; πa^2 is the water plane area inside the cylinder.

$\omega_n = \sqrt{\frac{g}{b+0.5a}}$ is close to Faltinsen's (1990) approximation of the natural frequency when b/a is large enough.

Set the radius a=3 ft; and the draft b=5 ft; for a water depth h= 20 ft; and incident wave height H_{inc}=0.7 ft. The incident wave frequency ω is varied. Table 7 and Figure 6 show a sample calculation result for wave height transfer ratio.

Table 7: Wave height transfer ratio (Case 1)

ω	0.5	1	1.5	1.8	2	2.1
ω^2h/g	0.155	0.622	1.399	2.014	2.486	2.741
H_{OWC}/H_{inc}	1.002	1.014	1.085	1.300	1.877	2.891
ω	2.3	2.4	2.5	2.8	3	3.2
ω^2h/g	3.288	3.581	3.885	4.874	5.595	6.365
H_{OWC}/H_{inc}	2.794	1.179	0.654	0.186	0.093	0.049

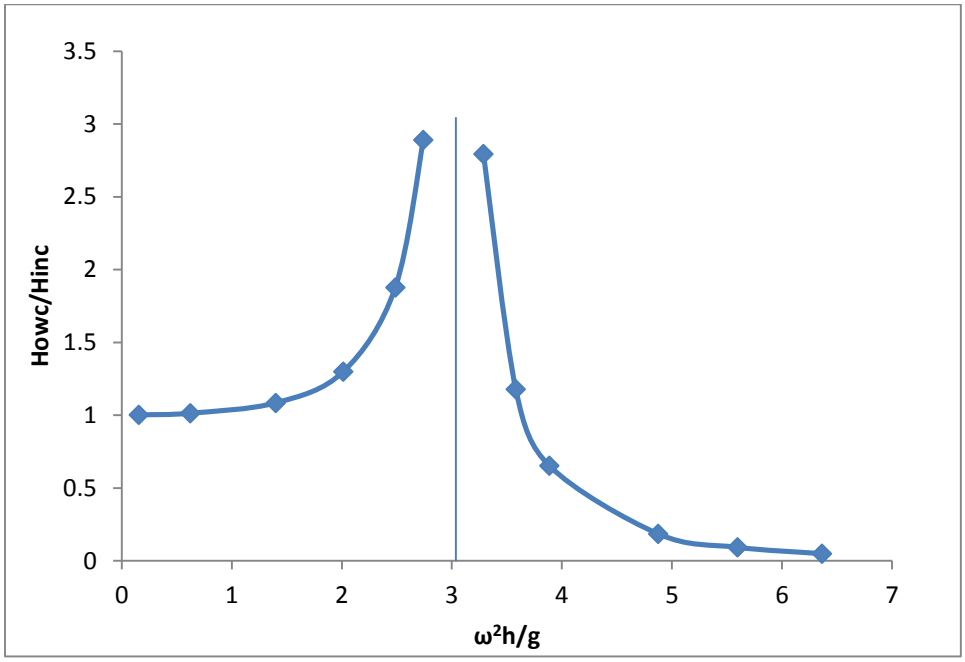

Figure 6. Wave height transfer ratio when a=3 ft, b=5ft

$\omega_n = \sqrt{\frac{g}{b+0.5a}} = 2.22\ rad/s$.The nondimensional natural frequency is 3.077, which matches the numerical result.

When the draft is slightly changed from 5ft to 8ft, the response is also changing. Set the radius a=3 ft; the draft b=8 ft; the water depth h= 20 ft; and the incident wave

height H_{inc}=0.7 ft. The incident wave frequency ω is varied. Table 8 and Figure 7 show the result for wave height transfer ratio:

Table 8: Wave height transfer ratio (Case 2)

ω	0.5	1	1.5	1.6	1.7	1.72
ω^2h/g	0.155	0.622	1.399	1.591	1.796	1.839
H_{OWC}/H_{inc}	1.007	1.048	1.381	1.681	2.491	2.835
ω	1.9	2	2.2	2.4	2.6	2.8
ω^2h/g	2.244	2.486	3.009	3.581	4.202	4.874
H_{OWC}/H_{inc}	2.875	1.002	0.296	0.118	0.052	0.024

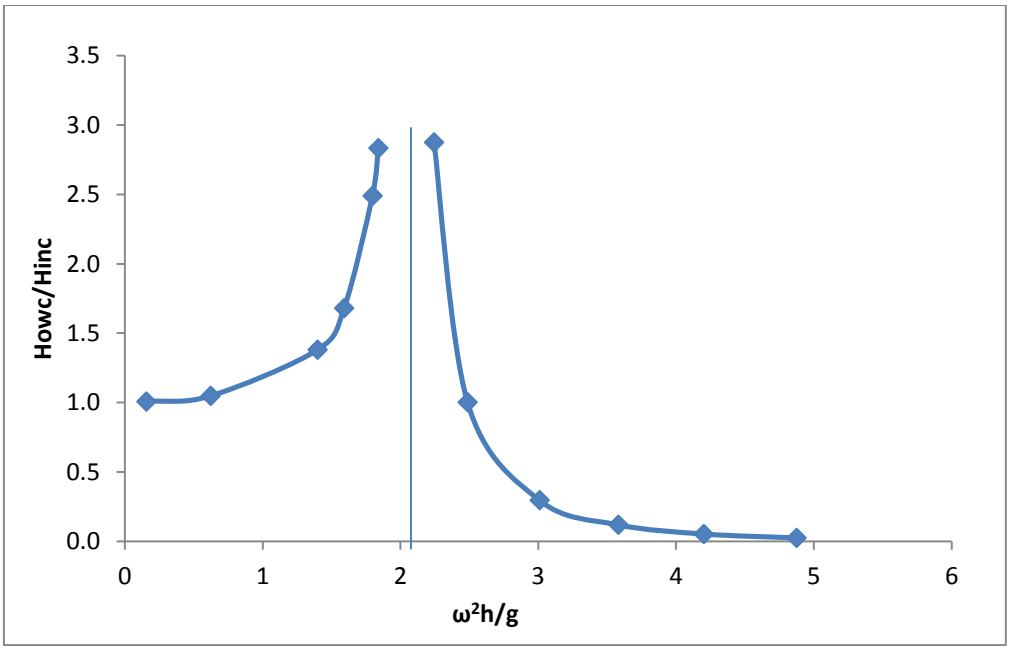

Figure 7. Wave height transfer ratio when a=3 ft, b=8 ft

$\omega_n = \sqrt{\frac{g}{b+0.5a}} = 1.84\ rad/s$, the nondimensional natural frequency is 2.105, which matches the numerical result. We can find the natural frequency decreases as the draft increases.

The response is also changing when we change the radius of the cylinder. Set the radius a=4.8 ft; the draft b=5 ft; the water depth h= 20 ft; the incident wave height H_{inc}=0.7 ft. The incident wave frequency ω is varied. Table 9 and Figure 8 show the result for wave height transfer ratio:

Table 9: Wave height transfer ratio (Case 3)

ω	0.5	1	1.5	1.8	2	2.05
ω^2h/g	0.155	0.622	1.399	2.014	2.486	2.612
H_{OWC}/H_{inc}	1.003	1.019	1.123	1.482	2.729	3.490
ω	2.2	2.3	2.4	2.6	2.8	3
ω^2h/g	3.009	3.288	3.581	4.202	4.874	5.595
H_{OWC}/H_{inc}	1.927	0.958	0.559	0.240	0.119	0.063

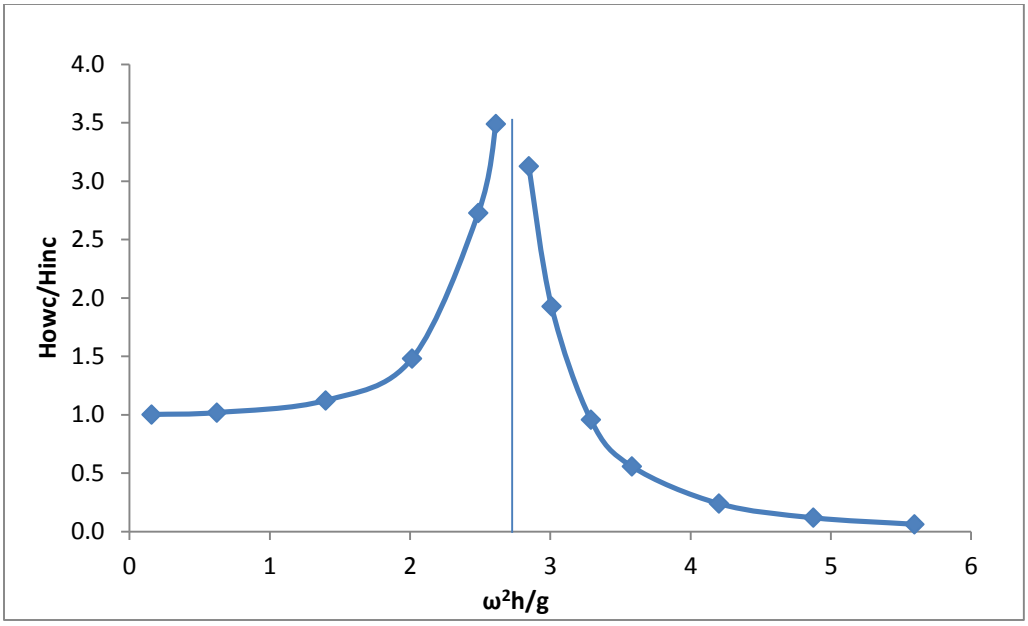

Figure 8. Wave height transfer ratio when a=4.8 ft, b=5 ft

$\omega_n = \sqrt{\frac{g}{b+0.5a}} = 2.085\ rad/s$, the nondimensional natural frequency ${\omega_n}^2 h/g$ is 2.703, which matches numerical result. We can find the natural frequency decreases as the radius increases.

Table 10 and Figure 9 show how the natural frequency is determined by the draft. Set the radius a=3 ft; the draft b=5 ft; the water depth h= 100 ft; and the incident wave height H_{inc}=0.7 ft. When we change only the draft and calculate the natural frequency, we can get the following results:

Table 10: Natural frequency with respect to the draft

b (ft)	Predicted	Nondimensional	Numerical	Nondimensional
5	2.225	15.385	2.220	15.318
10	1.673	8.699	1.670	8.668
15	1.396	6.057	1.390	6.005
20	1.223	4.649	1.220	4.626
25	1.102	3.774	1.100	3.761
30	1.011	3.177	1.000	3.108

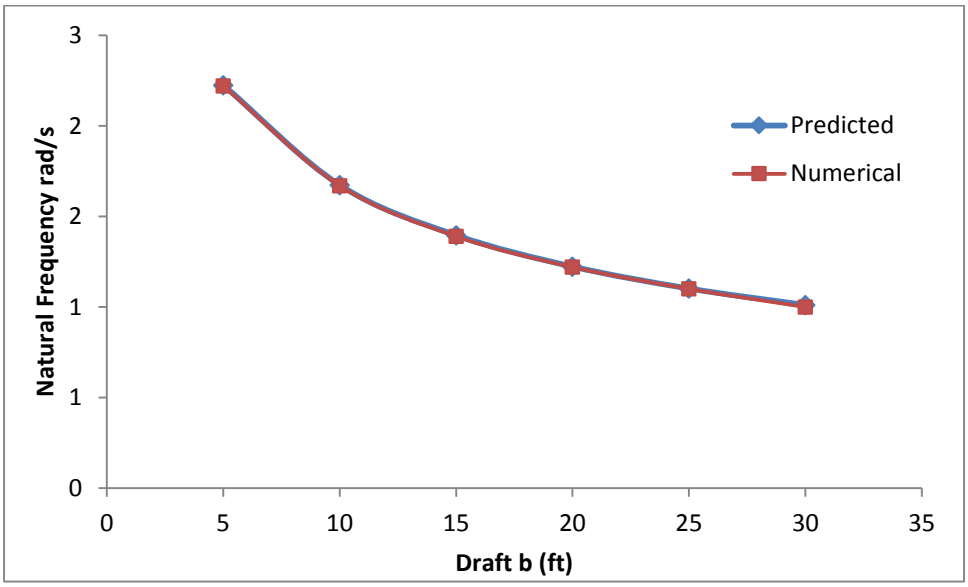

Figure 9. Natural frequency with respect to draft of the cylinder

The result from the model perfectly matches the prediction.

When we set b=10ft and change only the radius of the cylinder, the natural frequency is shown in Table 11 and Figure 10:

Table 11: Natural frequency with respect to the radius

a (ft)	Predicted	Nondimensional	Numerical	Nondimensional
1	1.750	9.519	1.740	9.410
2	1.710	9.088	1.705	9.035
4	1.637	8.329	1.634	8.298
6	1.573	7.690	1.571	7.671
8	1.516	7.143	1.515	7.134
10	1.465	6.671	1.468	6.698

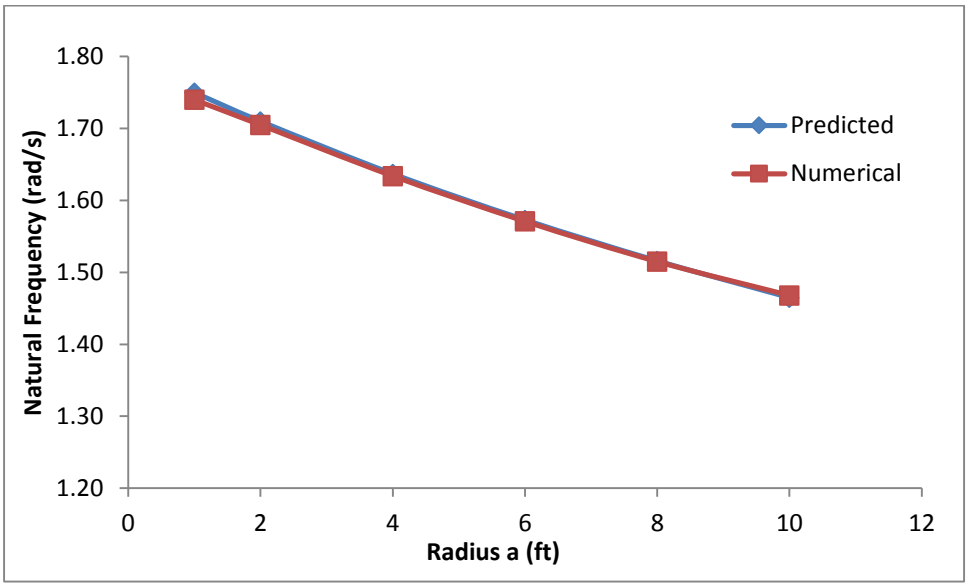

Figure 10. Natural frequency with respect to the radius of the cylinder

In the calculation above, we can observe that the natural frequency (the frequency when $\frac{H_{OWC}}{H_{inc}}$ has very large value) matches the equation $\omega_n = \sqrt{\frac{g}{b+0.5a}}$. In future calculations, we can use this equation to estimate the natural frequency effectively.

In the following, the effect of water depth on the natural frequency is studied.

We set the radius a= 3 ft, the draft b=10 ft and run the computer program OWC Solution for a given water depth to find the natural frequency corresponding to each water depth. The results are given in Table 12 and Figure 11:

Table 12: Natural frequency with respect to water depth

h (ft)	ω_n(rad/s)	h (ft)	ω_n(rad/s)
100	1.670	14	1.650
80	1.670	13	1.640
60	1.670	12	1.620
40	1.670	11	1.580
30	1.669	10.5	1.520
20	1.668	10.3	1.470
15	1.660	10.1	1.400

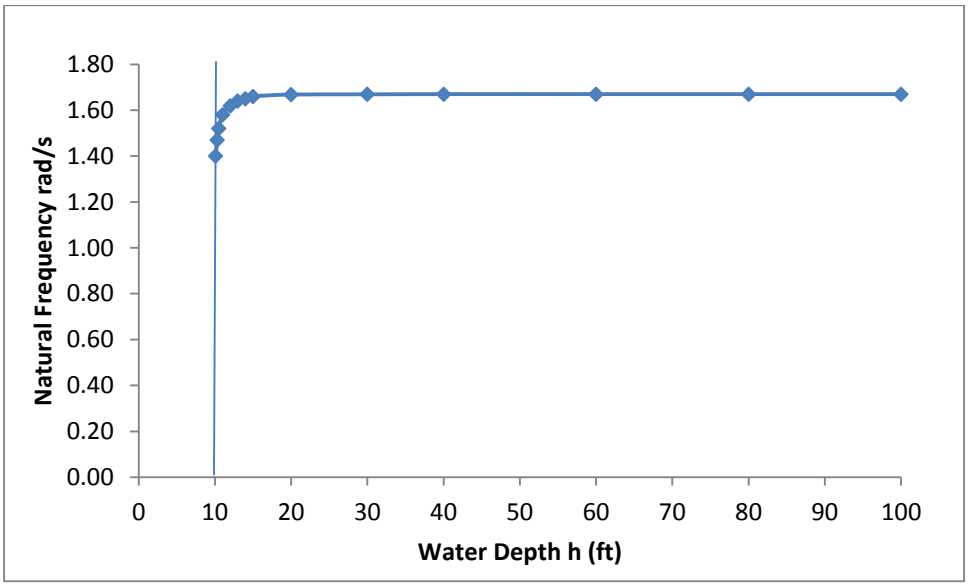

Figure 11. Natural frequency with respect to water depth

Calculations of the natural frequency as a function of water depth h show that the natural frequency is basically not affected by the water depth. However, as b/h comes close to 1, the natural frequency will decrease, which indicates the bottom effect.

3.6 Geometric Parameters Effect on the Response Amplitude Operator

The following calculations show us how the response inside the cylinder is affected by certain geometric parameter, when you fix other parameters.

Initial value: a= 1ft; b=25ft; h=50ft; ω= 1 rad/s. We change only the radius of the cylinder to see how the radius affects the wave amplitude inside the cylinder. The results are shown in Table 13 and Figure 12:

Table 13: Wave height transfer function with respect to radius

a (ft)	H_{OWC}/H_{inc}	a (ft)	H_{OWC}/H_{inc}
1	1.863	11	6.663
3	2.164	12	7.725
5	2.607	13	7.813
7	3.312	14	6.770
9	4.538	16	4.393
10	5.483	18	3.015

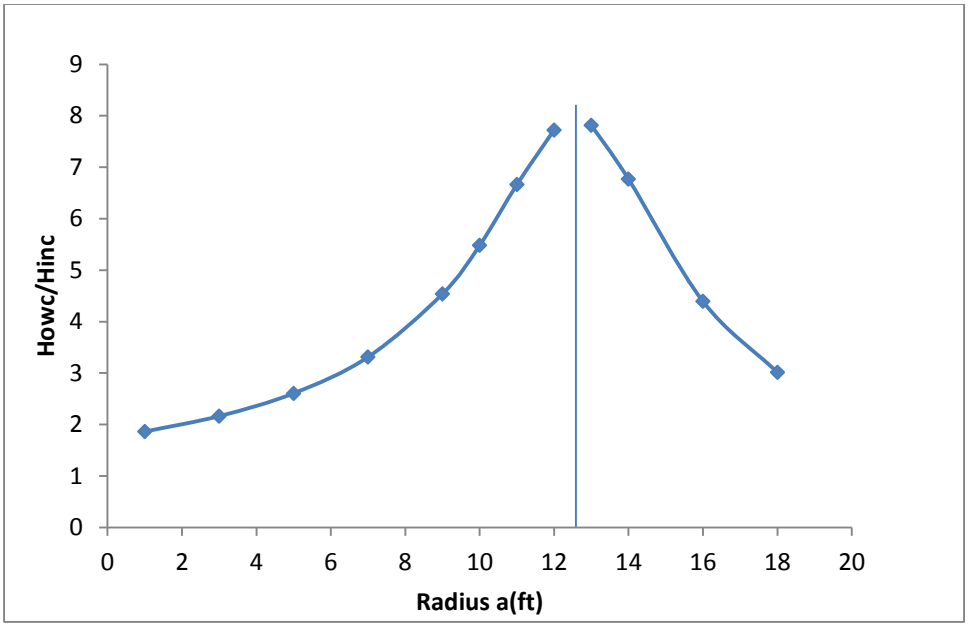

Figure 12. Wave height transfer ratio with respect to the radius of the cylinder

We can observe that the RAO reaches peak when a=12.5 ft, $\omega_n =$ $\sqrt{\frac{32.174}{25+12.5/2}}$ =1.015 rad/s, which is very close to the incident wave frequency.

We change only the draft of the cylinder to see how the draft affects the response inside the cylinder. The results are shown in Table 14 and Figure 13:

Table 14: Wave height transfer ratio with respect to draft

b(ft)	H_{OWC}/H_{inc}	b(ft)	H_{OWC}/H_{inc}
20	1.290	30	6.453
22	1.440	33	6.451
24	1.682	35	2.522
26	2.114	37	1.506
28	3.058	38	1.239

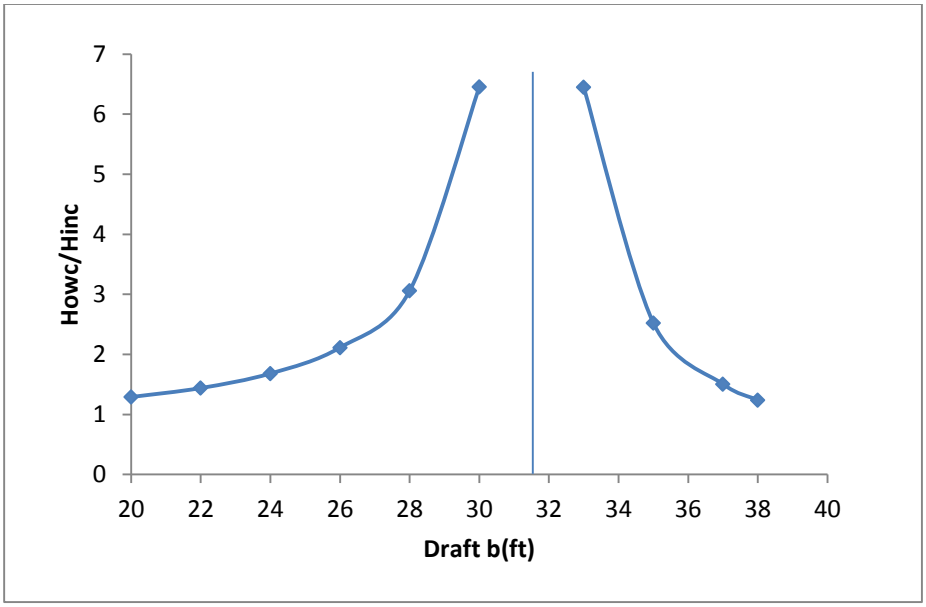

Figure 13. Wave height transfer ratio with respect to the draft of the cylinder

It can be observed that the RAO reaches peak when b=31.5 ft, $\omega_n = 1.003\ rad/s$, which is very close to the incident wave frequency (1 rad/s).

We change only the water depth to see how the water depth affects the response inside the cylinder. The results are shown in Table 15 and Figure 14:

Table 15: Wave height transfer ratio with respect to water depth

h(ft)	H_{OWC}/H_{inc}	h(ft)	H_{OWC}/H_{inc}
100	1.781	60	1.810
90	1.780	50	1.863
80	1.781	40	1.989
70	1.788	30	2.297
65	1.796	28	2.410

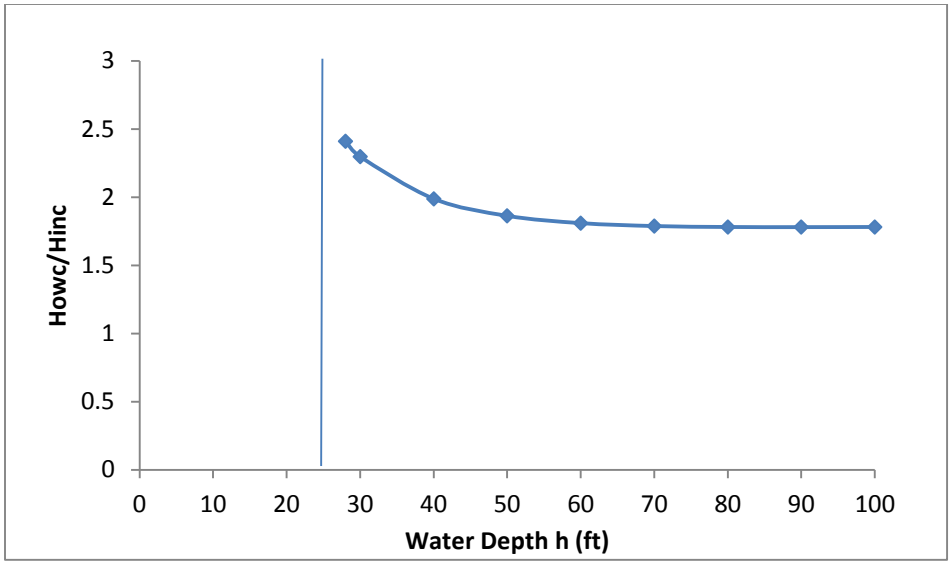

Figure 14. Wave height transfer ratio with respect to the water depth

The draft of the cylinder b=25 acts like a wall to the RAO curve. The RAO over the water depth indicates the bottom effect of the system: when the draft of the cylinder becomes close to the water depth, the response inside the cylinder will be significantly affected by the bottom.

The calculations of RAO with respect to geometric parameters will be very useful for OWC system design in the following process:

(1) Analyze the dominant incident wave frequency (wave frequency corresponding to the peak of the wave spectrum);

(2) Set the natural frequency as (or close) to the incident wave frequency.

(3) Follow $\omega_n = \sqrt{\frac{g}{b+a/2}}$ to approximately select the radius and draft of the cylinder. Usually, the draft can be adjusted more easily.

(4) Calculate the response inside the cylinder using the VBA program called OWC Solution.

3.7 Scattering Volume Flux inside the Cylinder

Corresponding to the incident wave height H_{inc}, the incident wave potential is:

$$\Phi_{inc} = Re\{\sum_{q=0}^{\infty} \epsilon_q \, i^q J_q(kr)\cos(q\theta)\psi_0(y)\, e^{-i\omega t}\} \cdot \frac{H_{inc}}{2} \cdot \frac{g}{w} \cdot \frac{1}{\psi_0(y)\,\big|_{y=0}} i$$

So the scattering volume flux across the surface is:

$$Q^S = \frac{H_{inc}}{2} \cdot \frac{g}{w} \cdot \frac{1}{\psi_0(y)\,\big|_{y=0}} i \cdot \frac{4\pi ikahJ_1(ka)S_{21}}{\pi kakhJ_1(ka)H_1(ka) + 2iS_{22}}$$

If we define the phase of wave elevation at the center of cylinder as zero, then the phase of the scattering volume flux is:

$$\theta_{Q^S} = arctan[\frac{Im(Q^S)}{Re(Q^S)}]$$

Table 16 and Figure 15 show the scattering volume flux with respect to the incident wave frequency. Set a= 1ft; b=25ft; h=65ft; we only change the incident wave frequency:

Table 16: Volume flux magnitude and phase angle over the frequency domain

ω	ω^2h/g	Q^S	θq	ω	ω^2h/g	Q^S	θq
0.5	0.505	1.243	-90.000	1.17	2.766	10.645	89.701
0.6	0.727	1.546	-90.000	1.2	2.909	6.289	89.775
0.75	1.136	2.139	-89.998	1.3	3.414	2.340	89.819
0.9	1.636	3.266	-89.991	1.4	3.960	1.245	89.801
1	2.020	5.387	-89.963	1.5	4.546	0.747	89.760
1.05	2.227	8.630	-89.910	1.7	5.839	0.308	89.633
1.065	2.291	10.723	-89.873	2	8.081	0.089	89.318

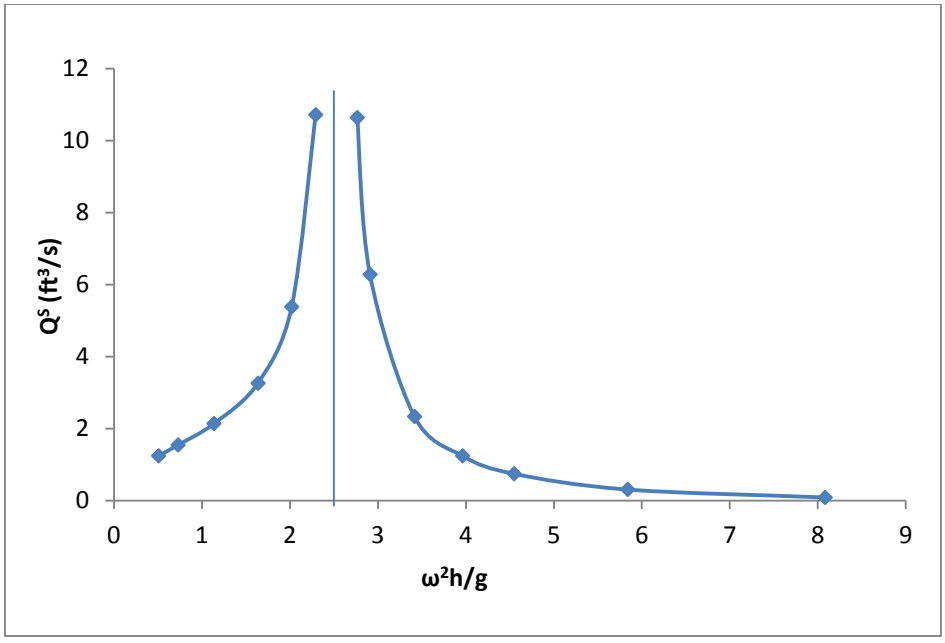

Figure 15. Scattering induced volume flux with respect to frequency

Using the natural frequency equation $\omega_n = \sqrt{\frac{32.174}{25+\frac{1}{2}}} = 1.123$ rad/s; ${\omega_n}^2 h/g = 2.549$. We can observe that the volume fluxes have large values near the natural frequency and it have a similar curve with the H_{OWC}/H_{inc} curve, but it do not decrease as quickly as the H_{OWC}/H_{inc} curve after the natural frequency because frequency itself contributes to the volume flux.

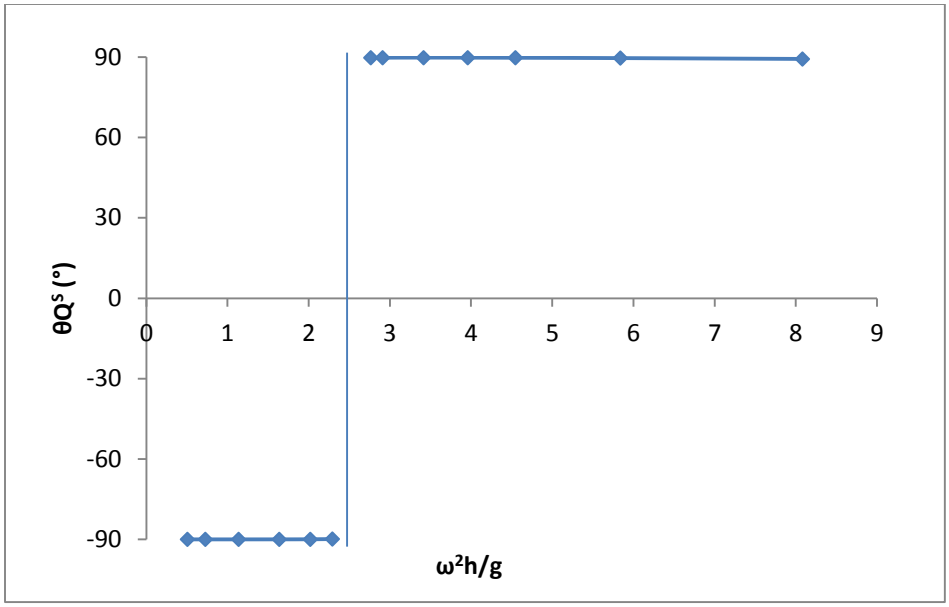

Figure 16. Scattering volume flux phase angle with respect to frequency

Figure 16 shows the scattering volume flux phase angle, which changes its positive/negative sign over the natural frequency.

3.8 Fluid Motion inside the Cylinder

In subsection 3.4, we have studied the free surface elevation at the center of the cylinder. However, the fluid motion inside the cylinder is not uniform across the water plane inside the cylinder. The following is the free surface elevation profile across the horizontal plane inside the cylinder.

Set the radius a=2 ft; the draft b=10 ft; the water depth h= 40 ft; the incident wave frequency ω=1 rad/s; the incident wave height H_{inc}=0.7 ft. Table 17 and Figure 17 show the wave height with respect to transverse coordinate:

Table 17: Wave height in transverse coordinate

r (ft)	H_{OWC}	r (ft)	H_{OWC}
0	0.725670	-2	0.724832
0.5	0.725610	-1.5	0.725190
1	0.725450	-1	0.725450
1.5	0.725190	-0.5	0.725610
2	0.724832	0	0.725670

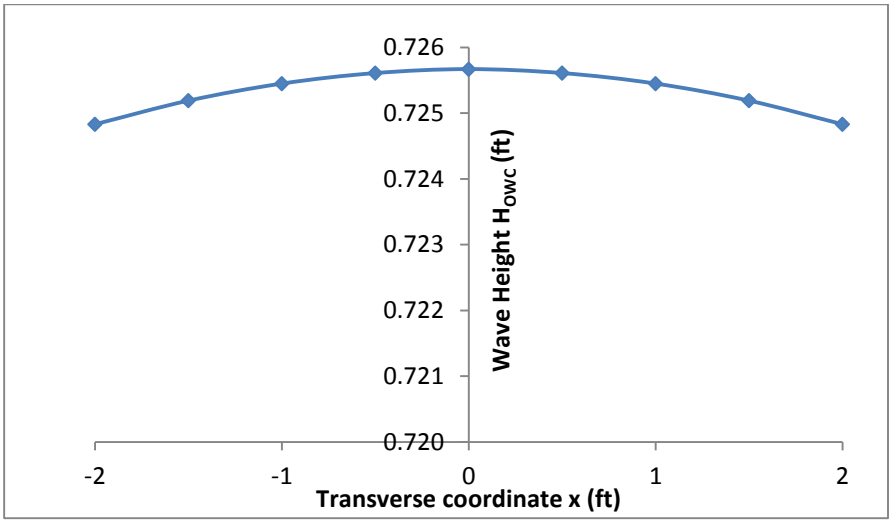

Figure 17. Wave height profile in transverse coordinate

We can notice that the wave height at different points inside the cylinder is quite close (0.12% difference). The center of the cylinder has the highest wave height and the wave height decreases as it comes closer to the radius of the cylinder.

Longitudinal wave height distribution is shown in Table 18 and Figure 18:

Table 18: Wave height in longitudinal coordinate

z (ft)	H_{OWC} (ft)	z (ft)	H_{OWC} (ft)
-2	0.72527	0	0.72567
-1.5	0.72545	0.5	0.72565
-1	0.72557	1	0.72557
-0.5	0.72565	1.5	0.72545
0	0.72567	2	0.72527

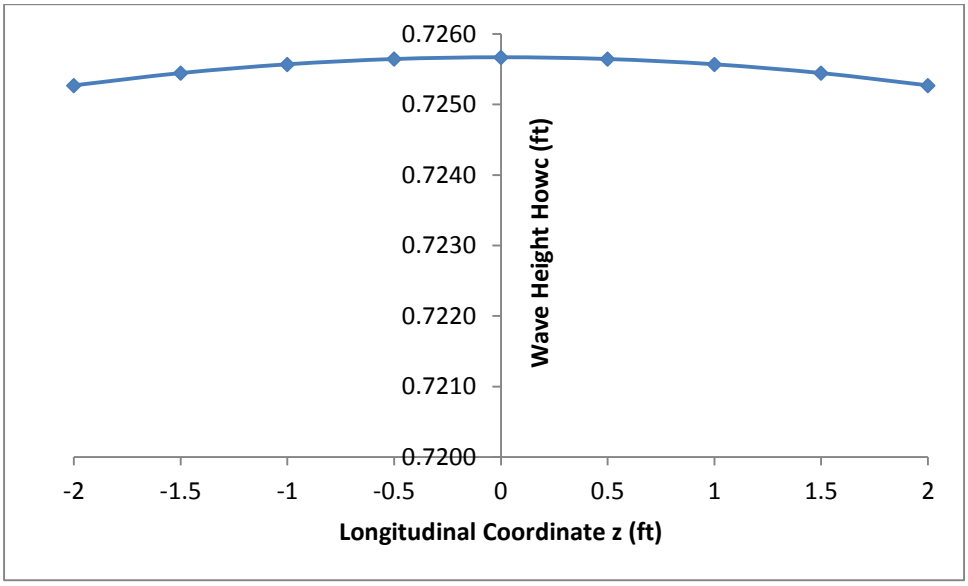

Figure 18. Wave height profile in longitudinal coordinate

The wave height distribution with respect to the angular coordinate is given in Table 19 and Figure 19. The distance from a point C on the curve to the origin represents the wave height at the angular coordinate of C.

Table 19: Wave height in angular coordinate

θ	H_{OWC}	θ	H_{OWC}
0	0.724832	180	0.724915
30	0.724937	210	0.725009
60	0.725151	240	0.725193
90	0.725271	270	0.725271
120	0.725193	300	0.725151
150	0.725009	330	0.724937

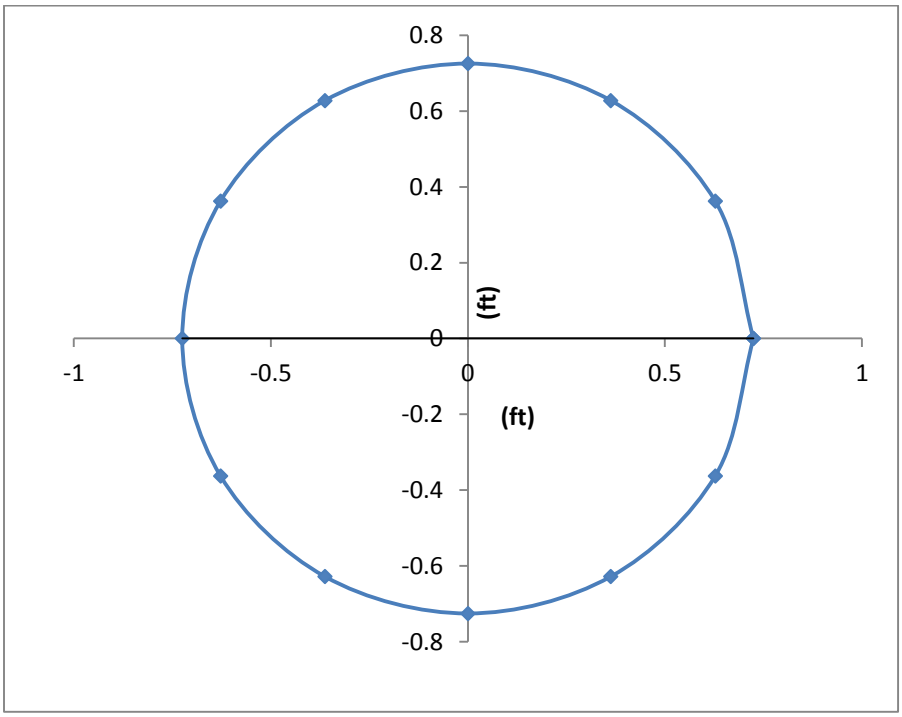

Figure 19. Wave height profile in angular coordinate

Table 20 and Figure 20 show the velocity magnitude calculated conveniently from the equation:

$$|V(r,\theta)| = \frac{\omega H_{OWC}(r,\theta)}{2}$$

Table 20: Vertical velocity magnitude in transverse coordinate

r (ft)	|V|	r (ft)	|V|
-2	0.36242	0	0.36284
-1.5	0.3626	0.5	0.36281
-1	0.36273	1	0.36273
-0.5	0.36281	1.5	0.3626
0	0.36284	2	0.36242

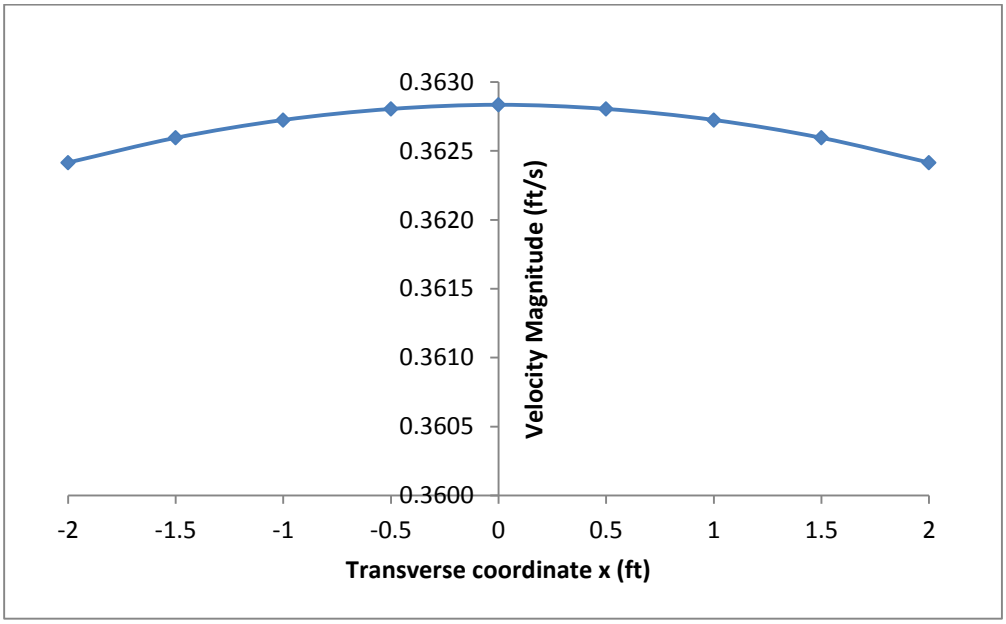

Figure 20. Velocity magnitude profile in transverse coordinate

We can find that the vertical velocity at different points inside the cylinder is quite close. The center of the cylinder has the highest vertical velocity and the vertical velocity decreases as it comes closer to the radius of the cylinder. Similarly, you can get the vertical velocity profile with respect to the longitudinal coordinate and angular

coordinate. In Table 21, numerical integration is used to calculate the scattering volume flux:

Table 21: Calculate scattering volume flux using numerical integration

r/a	Re(V)	Im(V)	|V|	dS	dQ^S
0	0.362835	0.000051	0.362835	0.000000	0
0.05	0.362832	0.000783	0.362834	0.031416	0.011399
0.1	0.362826	0.001514	0.362832	0.094248	0.034196
0.15	0.362816	0.002246	0.362828	0.157080	0.056991
0.2	0.362803	0.002977	0.362823	0.219911	0.079784
0.25	0.362786	0.003709	0.362816	0.282743	0.102575
0.3	0.362766	0.004440	0.362808	0.345575	0.125363
0.35	0.362742	0.005172	0.362798	0.408407	0.148146
0.4	0.362715	0.005903	0.362787	0.471239	0.170925
0.45	0.362684	0.006634	0.362774	0.534071	0.193699
0.5	0.362650	0.007365	0.362760	0.596903	0.216467
0.55	0.362613	0.008096	0.362745	0.659734	0.239228
0.6	0.362572	0.008827	0.362727	0.722566	0.261982
0.65	0.362527	0.009558	0.362709	0.785398	0.284728
0.7	0.362479	0.010289	0.362689	0.848230	0.307466
0.75	0.362428	0.011020	0.362667	0.911062	0.330194
0.8	0.362373	0.011750	0.362644	0.973894	0.352913
0.85	0.362315	0.012481	0.362619	1.036726	0.375621
0.9	0.362253	0.013211	0.362593	1.099557	0.398318
0.95	0.362187	0.013941	0.362565	1.162389	0.421003
1	0.362119	0.014671	0.362536	1.225221	0.443676
SUM				12.566371	4.554673

Notice that the area of the cross section of the cylinder is $\pi \cdot 2^2 = 12.566371\,\text{ft}^2$. The volume flux given by the computer program OWC Solution is 4.843438 ft^3/s. So the numerical integration is 94.04% compared to the result given by Evans model.

Remind that the Re(V)/ |V| is greater than 0.9988, so even if we approximate the vertical velocity with only a slightly smaller velocity at time instant t=0,which is very close to the peak instant at t=0.0001 s, the error should be smaller than 0.12%. Considering that the higher order disturbances are not taken into account for the numerical integration, this is a reasonable result.

4. THE RADIATION PROBLEM

4.1 The Solution for the Hydrodynamic Coefficients in Radiation

The radiation problem concerns itself with the fluid motion when there is no incident wave, but oscillating air pressure exists on the water column inside the cylinder.

The solution for the radiation problem in this subsection was derived by Evans and Porter (1997).

Corresponding to air pressure oscillation amplitude p with frequency ω, outside the cylinder:

$$\phi^R = \alpha_0^R H_0(kr)\psi_0(y) + \sum_{n=1}^{\infty} \alpha_n^R K_0(k_n r)\psi_n(y)$$

Inside the cylinder:

$$\phi^R = \beta_0^R J_0(kr)\psi_0(y) + \sum_{n=1}^{\infty} \beta_n^R I_0(k_n r)\psi_n(y) + g/\omega^2$$

α_0^R and β_0^R are the coefficients for the radiation wave potential, where α_n^R and β_n^R are coefficients for higher order terms. If we define:

$$U^R(y) = \frac{\partial \phi^R}{\partial r}|_{r=a}$$

Based on continuity of the radial velocity at the radius of the cylinder, we can achieve the relationship between the hrodynamic coefficients for the potential inside and outside the cylinder:

$$\alpha_0^R k H_0'(ka) = \beta_0^R k J_0'(ka) = \frac{1}{h}\int_b^h U^R(y)\psi_0(y)\,dy$$

$$\alpha_i^R k_i K_0'(k_i a) = \beta_i^R k_i I_0'(k_i a) = \frac{1}{h}\int_b^h U^R(y)\psi_i(y)\,dy$$

In addition, the fluid potential is continuous at the radius of the cylinder. So we can get another equation between the coefficients of wave potential inside and outside the cylinder:

$$\alpha_0^R H_0(ka)\psi_0(y) + \sum_{i=1}^{\infty} \alpha_i^R K_0(k_n a)\psi_i(y)$$

$$= \beta_0^R J_0(ka)\psi_0(y) + \sum_{i=1}^{\infty} \beta_i^R I_0(k_i a)\psi_i(y) + \frac{g}{\omega^2}$$

Applying the Wronskian identities for Bessel functions:

$$\int_b^h U^R(l)L_0(y,l)dl = -\frac{g}{\omega^2} + \frac{2i\alpha_0^R}{\pi ka J_1(ka)}\psi_0(y)$$

Evans and Porter (1997) set:

$$U^R(y) = -\frac{g}{\omega^2}u_1(y) + \frac{2i\alpha_0^R}{\pi ka J_1(ka)}u_2(y)$$

So:

$$\alpha_0^R k H_0'(ka) = \frac{1}{h}\int_b^h [-\frac{g}{\omega^2}u_1(y) + \frac{2i\alpha_0^R}{\pi ka J_1(ka)}u_2(y)]\psi_0(y)\,dy$$

The radiation induced volume flux across the free surface is:

$$q^R = -\int_b^h \int_0^{2\pi} U^R(y) a d\theta dy$$

According to the result given by the Galerkin Approximation in subsection 3.2:

$$\alpha_0^R = \frac{\frac{g}{\omega^2}\pi ka J_1(ka) S_{12}}{\pi kakh J_1(ka) H_1(ka) + 2iS_{22}}$$

$$q^R = \frac{2\pi \frac{g}{\omega^2} a[\pi kakhJ_1(ka)H_1(ka)S_{11} + 2i(S_{11}S_{22} - S_{12}S_{21})]}{\pi kakhJ_1(ka)H_1(ka) + 2iS_{22}}$$

4.2 Magnitude of the Radiated Wave Power

According to Evans and Porter (1997), we can measure the magnitude at the far-field using the following equation:

$$\phi^R \sim \alpha_0^R H_0(kr)\psi_0(y)$$

According to Abramowizt and Stegun (1964), when r is large:

$$H_0(kr) \sim (\frac{2}{\pi kr})^{1/2} e^{ikr - i\pi/4}$$

We can calculate the magnitude of the radiated waves at the far field when r is large.

$$\Phi^R = \frac{i\omega p}{\rho g} \alpha_0^R (\frac{2}{\pi kr})^{1/2} e^{ikr - i\pi/4} \psi_0(y) e^{-i\omega t}, \qquad r \geq a$$

The radiated wave height at r from the center of the cylinder is:

$$H_R = \left| \frac{2}{g} \frac{\omega^2 p}{\rho g} \alpha_0^R \left(\frac{2}{\pi kr}\right)^{\frac{1}{2}} e^{ikr - \frac{i\pi}{4}} \psi_0(y)|_{y=0} \right|$$

The radiated wave is angularly symmetric so it has the same amplitude with respect to the angular coordinate θ. The radiated power can be calculated as:

$$P_r = \left(\frac{1}{8}\rho g {H_R}^2\right) \frac{\omega}{k} [\frac{1}{2}(1 + \frac{2kh}{sinh(2kh)})] \cdot (2\pi r)$$

The radiated power can be also calculated according to the radiation volume flux:

$$P_r = \frac{1}{T} \int_0^T p_e \frac{iwp}{\rho g} q^R dt$$

We will find that two ways of calculating the radiated power give the same result.

4.3 Results and Discussion about the Radiation Problem

Table 22 and Figure 21 show a case of solving radiation problem:

Table 22: Sample case of a radiated wave

ω	1.5 rad/s	a	4 ft
h	30 ft	b	10 ft
	Real	Imaginary	
C_t	10	0	$(ft^3/s)/(lbf/ft^2)$
p	-10.160	11.577	psf
Q_R	-79.763	-92.642	ft^3/s

The radiation coefficients we solved for this case is:$\alpha_0^R = 0.177 - 2.363i$, $\beta_0^R = -39.263 - 5.317i$. The radiated wave height at r from the center of the axis is:

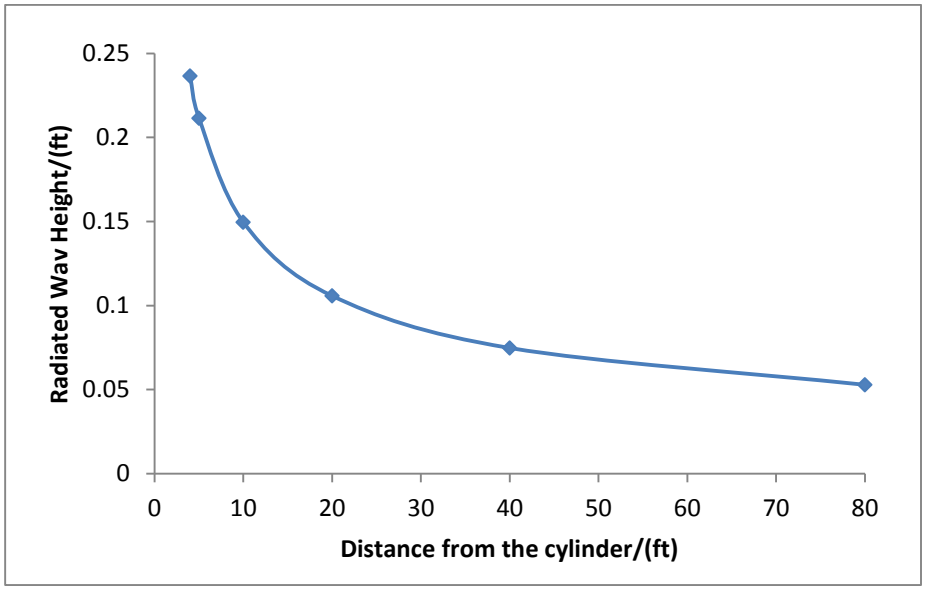

Figure 21. Radiated wave height with respect to distance from the cylinder

The radiated wave power is uniform no matter how far you measure it: 177.68 Watt.

We can calculate the radiation induced volume flux inside the cylinder with respect to pressure variation as shown in Table 23 and Figure 22. Set ω= 1.05 rad/s; a=2 ft; b=25 ft; h=65 ft:

Table 23: Radiation volume flux with respect to pressure variation

p(psf)	Qr (ft^3/s)	p (psf)	Qr (ft^3/s)
14.875	29.843	2.001	4.014
13.932	27.951	1.341	2.690
9.947	19.957	1.008	2.022
7.079	14.202	0.505	1.013
6.118	12.274	0.253	0.507
4.772	9.574	0.135	0.270
3.893	7.810	0.051	0.101
2.648	5.312	0.020	0.041

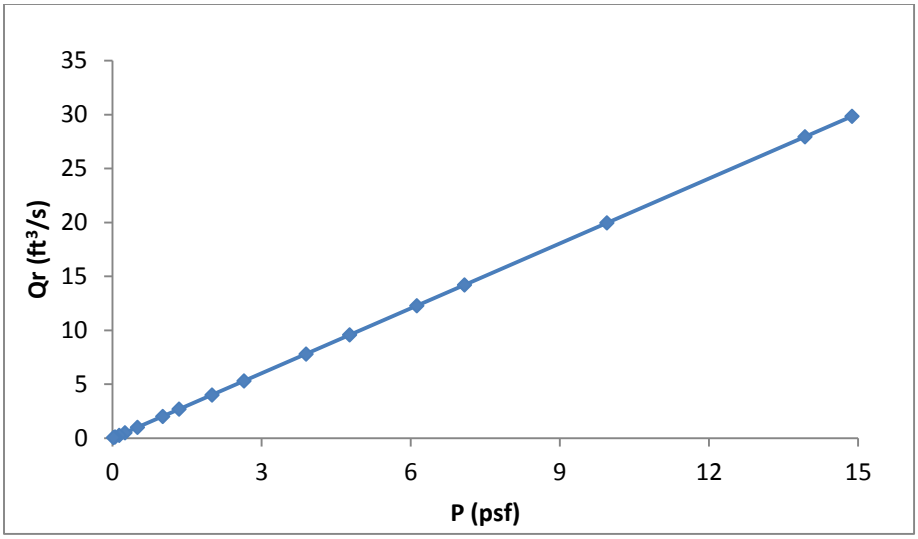

Figure 22. Radiation volume flux with respect to pressure variation

Obviously, the radiation volume flux is proportional to the pressure variation magnitude above the free surface. The following is the radiation volume flux in the frequency domain, as shown in Table 24 and Figure 23. Set p=20.224 psf; a=2 ft; b=25 ft; h=65 ft:

Table 24: Radiation volume flux with respect to frequency

ω	Qr (ft^3/s)	ω	Qr (ft^3/s)
0.5	1.718	1.2	19.127
0.7	3.187	1.3	9.485
0.9	7.230	1.4	6.441
1	14.701	1.5	4.940
1.05	27.951	1.7	3.441
1.17	28.120	2	2.426

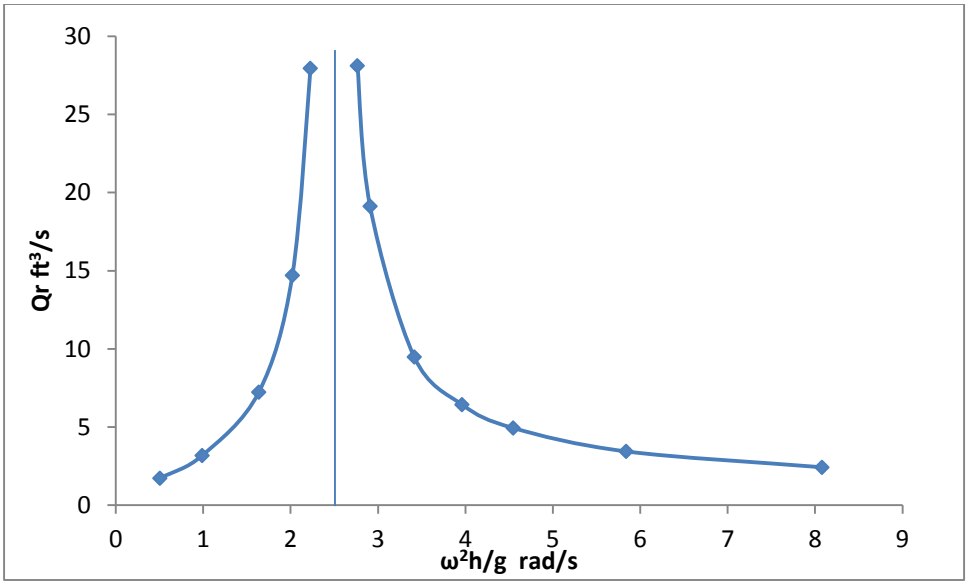

Figure 23. Radiation volume flux with respect to frequency

The radiated waves have the same natural frequency as the scattered waves for a given cylinder, which can be calculated by: $\omega_n = \sqrt{\frac{32.174}{25+\frac{2}{2}}} = 1.112$ rad/s; ${\omega_n}^2 h/g$=2.500.

5. WAVE ENERGY ANALYSIS FROM AN OWC DEVICE

5.1 Model of Air Flow and Air Compression for the OWC System

The idea of the OWC device is extracting wave energy to generate electricity through an air turbine at the top of the cylinder. This involves the interaction between the air motion (determined by the air turbine, volume of the air chamber above the water surface and air compressibility) and water motion (determined by the incident wave and geometric parameters of the truncated vertical cylinder). The solution to the OWC system is a coupling of the scattering (incident and diffraction) and the radiation.

The derivation in this subsection is given according to derivation by Malmo and Reitan (1985) for an oscillating water column with square geometry.

We can divide the volume inside the cylinder into two parts: air volume and water volume. The change of water volume is due to the wave elevation inside the cylinder, since water is incompressible. We can define the water volume under the free surface inside the cylinder as V_η. The change of air volume is due to the air flow in/out the cylinder and the air compressibility. If we denote the air volume through the turbine by V_t, and denote the air volume inside the cylinder at certain pressure by V_p, the total air volume change inside the cylinder is: $V_p - V_t$, and V_0 is the volume of the cylinder.

$$V_\eta + V_p - V_t = V_0$$

Take the time derivative of both sides:

$$\frac{dV_\eta}{dt} - \frac{dV_t}{dt} = -\frac{dV_p}{dt}$$

In which $\frac{dV_\eta}{dt}$ is the water volume flux inside the cylinder; $\frac{dV_t}{dt}$ is the air flow rate through the turbine; $\frac{dV_p}{dt}$ is the compressing/depressing rate of the air inside the chamber;

The water volume flux is decomposed into two parts by Evans and Porter (1995):

$$\frac{dV_\eta}{dt} = q^S - \frac{i\omega p}{\rho g} q^R$$

q^S is the scattering volume flux across the horizontal plane inside the cylinder; $\frac{iwp}{\rho g} q^R$ is the radiation volume flux across the horizontal plane inside the cylinder. The radiation volume flux will generally decrease the scattering volume flux, which acts as damping to the water volume flux.

The air flow rate through the turbine is:

$$\frac{dV_t}{dt} = C_t \cdot p_e$$

This is a linearity assumption that the air flow rate through the turbine is proportional to the air pressure and turbine constant, which was suggested by Malmo and Reitan (1985). C_t is the turbine constant; which is a ratio between the air flow and the pressure drop through the turbine; p_e is the oscillating part of the air pressure. $(P(t) = p_a + p_e)$

Since the incident wave is time harmonic, the following terms are also time harmonic:

$$p_e = Re\left(p \cdot e^{-i\omega t}\right)$$

$$q^S = Re(Q^S \cdot e^{-i\omega t})$$

$$q^R = Re(Q^R \cdot e^{-i\omega t})$$

p, Q^S and $Q^R$is the complex magnitude of each variable. For given amount of air:

$$P \cdot {V_p}^k = C$$

C is a constant, k=1.4 for adiabatic process. Take the natural logarithm of both sides of the equation and then take the derivative of both sides:

$$\frac{dP}{P} + k\frac{dV_p}{V} = 0$$

The volume of air above the water surface can be written as $V = V_C + V_e(t)$, where V_C is the initial air chamber volume at calm state; $V_e(t)$ is the fluctuating part of the air chamber volume. So:

$$dV_p = -\frac{V_p dP}{kP}$$

We will make two linearity assumptions here, which are suggested by Malmo and Reitan (1985):

(1)$P(t) = p_a + p_e$, fluctuating air pressure p_e is very small compared with the atmosphere air pressure p_a;

(2) $V_p = V_C + V_e(t)$, fluctuating air chamber volume V_e is small compared with the original air chamber volume V_C.

$$dV_p = -\frac{V_C dp_e}{kP_a}$$

If we divide both sides by the time derivative dt:

$$\frac{dV_p}{dt} = -\frac{V_C}{kP_a} \cdot \frac{dp_e}{dt} = -\frac{V_C}{kP_a} \cdot (-i\omega) p e^{-i\omega t} = -\frac{V_C}{kp_a} \cdot p_e \cdot (-i\omega)$$

We can combine all the terms in the following equation:

$$q^S - \frac{i\omega p}{\rho g} q^R = C_t \cdot p_e + \frac{V_C}{k p_a} \cdot p_e \cdot (-i\omega)$$

We can remove the time dependence by dividing both sides by $e^{-i\omega t}$.

$$Q^S - \frac{i\omega p}{\rho g} Q^R = C_t \cdot p + \frac{V_C}{k p_a} \cdot p \cdot (-i\omega)$$

This is the equation that relates the hydrodynamics problem of open-top OWC to the air flow from a turbine-connected OWC system. There will be air pressure fluctuation above the water surface in the turbine-connected air chamber, which causes the radiation. This equation can be used to solve for oscillating air pressure and air flow through the turbine. Note that p, C_t, Q^S and Q^R is the complex magnitudes, so phases are also important in the air-water interaction. Table 25 is a sample OWC system:

Table 25: Input parameters for an air flow calculation case

ω	1.3	rad/s
h	100	ft
H_{inc}	1.5	ft
a	6	ft
b	20	ft
V_C	2000	ft^3
Ct-Real	Ct-Imaginary	-
9.36886	0.6	$(ft^3/s)/(lbf/ft^2)$

The flow from the given turbine is shown in Table 26:

Table 26 : Solution of an air flow calculation case

Pc	Real	Imaginary	|Pc|	θp
psf	-7.738	-5.922	9.744	-142.574°
Qt	Real	Imaginary	|Qt|	θq
ft^3/s	-68.942	-60.122	91.475	-138.910°

5.2 Energy Analysis

The energy input into this system is provided by the incident wave. According to Dean and Dalrymple (1984), the energy input rate is:

$$P_i = \left(\frac{1}{8}\rho g {H_{inc}}^2\right)\frac{\omega}{k}\left[\frac{1}{2}\left(1+\frac{2kh}{sinh(2kh)}\right)\right]\cdot(2a)$$

In which:

$$C_g = \frac{\omega}{k}\left[\frac{1}{2}\left(1+\frac{2kh}{sinh(2kh)}\right)\right]$$

C_g is the group velocity for the wave energy transmitting, and a is the radius of the cylinder. The air flow power driving the turbine is:

$$P_t = \frac{1}{T}\int_0^T Re\{[Re(p)+iIm(p)]e^{-i\omega t}\}Re\{[Re(Q_t)+iIm(Q_t)]e^{-i\omega t}\}dt$$

So:

$$P_t = \frac{1}{2}[Re(p)Re(Q_t)+Im(p)Im(Q_t)]$$

T is the period of the incident wave. $T = \frac{2\pi}{\omega}$.

The radiated power can be derived similarly:

$$P_r = \frac{1}{T}\int_0^T p_e \frac{iwp}{\rho g} q^R dt$$

So:

$$P_r = \frac{w}{\rho g} \cdot \frac{Im(p)[Re(q^R)Re(p) - Im(p)Im(q^R)]}{2}$$

$$+\frac{w}{\rho g} \cdot \frac{Re(p)[Re(p)Im(q^R) + Re(q^R)Im(p)]}{2}$$

$\frac{iwp}{\rho g} q^R$ is the radiation volume flux across the horizontal plane inside the cylinder; the radiation volume flux will lead to an energy dissipation from the OWC system.

The air compressibility does not do work through a complete time period because if we integrate the air compression induced volume change rate multiplied by the air pressure variation p_e:

$$P_{AC} = \frac{1}{T}\int_0^T \frac{V_C}{kp_a} \cdot p_e \cdot (-i\omega) \cdot p_e dt$$

$$P_{AC} = \frac{\omega}{T}\frac{V_C}{kp_a}\int_0^T Re\{[Re(p) + iIm(p)]e^{-i\omega t}\}Re\{[Im(p) - iRe(p)]e^{-i\omega t}\}dt$$

According to the orthogonal identity:

$$\int_0^T [\cos(\omega t)\, Re(p) + \sin(\omega t)\, Im(p)][\cos(\omega t)\, Im(p) - \sin(\omega t)\, Re(p)]dt = 0$$

So $P_{AC} = 0$.

The diffracted wave power is calculated according to the diffracted wave potential. According to the asymptotic expression for Hankel function, when kr is large:

$$H_0(kr) \sim (\frac{2}{\pi kr})^{1/2} e^{ikr - i\pi/4}$$

According to Evans and Porter (1997), the far-field diffracted wave potential is:

$$\phi^D \sim \sum_{q=0}^{\infty} \epsilon_q \, i^q cos(q\theta) \alpha_{q,0}^S \left(\frac{2}{\pi kr}\right)^{\frac{1}{2}} e^{ikr - \frac{i\pi}{4}} \psi_0(y)$$

Corresponding to the incident wave potential:

$$\Phi_{inc} = \frac{H_{inc}}{2} \cdot \frac{g}{w} \cdot \frac{1}{\psi_0(y)\,|_{y=0}} i \cdot \{\sum_{q=0}^{\infty} \epsilon_q \, i^q J_q(kr) \cos(q\theta) \psi_0(y) \, e^{-i\omega t}\}$$

The diffracted wave potential is:

$$\Phi^D = \frac{H_{inc}}{2} \cdot \frac{g}{w} \cdot \frac{1}{\psi_0(y)\,|_{y=0}} i \sum_{q=0}^{\infty} \epsilon_q \, i^q cosq\theta \alpha_{q,0}^S \left(\frac{2}{\pi kr}\right)^{\frac{1}{2}} e^{ikr - \frac{i\pi}{4}} \psi_0(y) e^{-i\omega t}$$

The diffracted wave height is:

$$H_d(r,\theta) = \frac{2}{g} \frac{\partial \Phi^D}{\partial t} = H_{inc} \cdot \sum_{q=0}^{\infty} \epsilon_q \, i^q \, cos(q\theta) \alpha_{q,0}^S \left(\frac{2}{\pi kr}\right)^{\frac{1}{2}} e^{ikr - \frac{i\pi}{4}} \psi_0(y)$$

$H_d(r,\theta)$ is the diffracted wave height at distance r from the center of the cylinder and at the angular coordinate θ. We can calculate the diffracted wave power when we integrate over the angular coordinate θ at radial coordinate r from the center.

$$P_d = \frac{1}{8} \rho g \frac{\omega}{k} \left[\frac{1}{2}\left(1 + \frac{2kh}{sinh(2kh)}\right)\right] \int_0^{2\pi} H_d(r,\theta)^2 \cdot r d\theta$$

The following is a sample case showing how the diffracted wave power changes in the frequency domain. The incident wave height H_{inc}=0.7 ft, the radius of the cylinder a=3 ft, the draft of the cylinder b= 6 ft, and the water depth h=40 ft. The diffracted wave power in the frequency domain is shown in Table 27 and Figure 24.

Table 27: Diffracted wave power respect to frequency

ω (rad/s)	0.5	1	1.5	1.7	1.85	1.9	2
ω^2h/g	0.311	1.243	2.797	3.593	4.255	4.488	4.973
RAO	1.001	1.011	1.124	1.343	1.841	2.224	4.623
P_i(Watt)	977.24	609.35	353.29	304.61	278.18	270.59	256.76
P_d(Watt)	0.00	0.09	1.72	5.06	14.57	25.32	189.56
ω	2.2	2.3	2.4	2.5	2.7	3	3.35
ω^2h/g	6.017	6.577	7.161	7.770	9.063	11.189	13.952
RAO	1.521	0.751	0.440	0.279	0.126	0.043	0.016
P_i(Watt)	233.25	223.09	213.79	205.23	190.03	171.03	155.48
P_d(Watt)	143.01	101.23	95.90	100.35	118.04	142.87	153.35

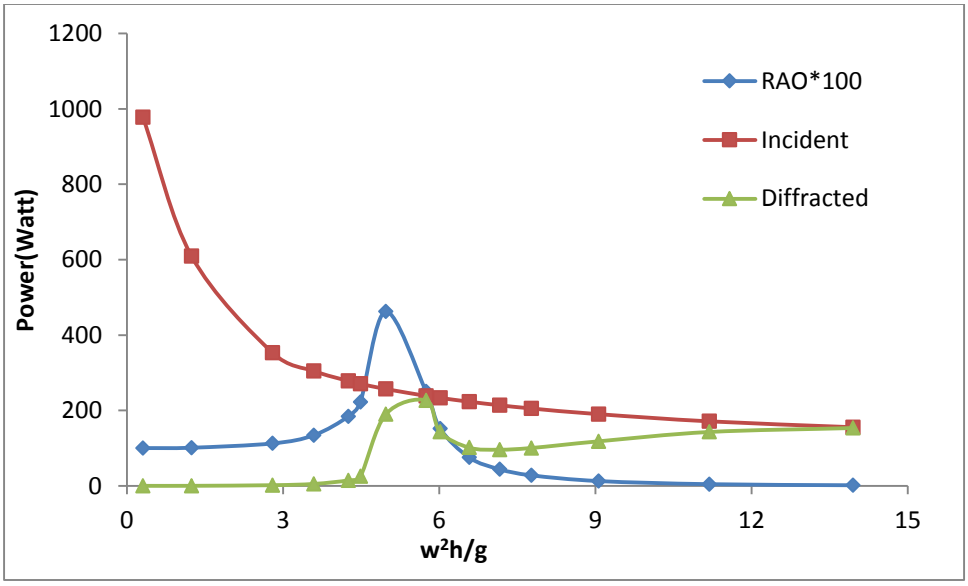

Figure 24. Diffracted and incident wave power with respect to frequency

The Response Amplitude Operator (RAO) here is represented by H_{OWC}/H_{inc}. At low frequency, the RAO is not much greater than 1, and the diffracted energy is very small. When the incident wave frequency gets close to the natural frequency; the diffracted wave power will reach large value. When it is very close to the natural

frequency, the diffracted power will exceed the incident power. However, we can still be confident about large RAOs that satisfy the energy balance in the model, we need to clarify that the results very close to the natural frequency are not reliable (for a very small part in the frequency domain). At higher frequency, the diffracted energy first decreases because the amplifying effect of the cylinder decreases at these frequencies; then the diffracted energy converges to the incident wave energy that almost all the wave energy is diffracted. So at high frequency, there is very small response inside the cylinder and very little energy entering the system.

As a conclusion, Evans and Porter's (1997) model works reasonably for most frequencies (except for the natural frequency). Using the model, you can get the hydrodynamic solution, linear air motion solution and the energy solution as in the following. Table 28, 29, 30 and 31 show a complete energy analysis case:

Table 28: Input parameters for sample energy analysis case

ω	1	rad/s
h	80	ft
H_{inc}	3	ft
a	8	ft
b	25	ft
V_C	12000	ft^3
Ct-Real	Ct-Imaginary	-
20	1	$(ft^3/s)/(lbf/ft^2)$

Table 29: Hydrodynamic solution for sample energy analysis case

k	0.031	k_1	0.029
k_2	0.074	k_3	0.114
Cg	16.918	T	6.283
λ	199.549	H_{OWC}/H_{inc}	4.584
-	Real	Imaginary	Magnitude
$VolumeFLux^S$	-162.75	1372.86	1382.47
$VolumeFLux^R$	-319.61	-1026.62	1075.22

Table 30: Motion analysis results for sample energy analysis case

Pc	Re	Im	|Pc|	θp
psf	-26.150	13.323	29.349	153.001
Qt	Re	Im	|Qt|	θq
ft^3/s	-536.329	240.318	587.709	155.864
Qt Difference		42.51%	dV/Vc	4.95%
Radiation Difference		77.78%	dp/Pa	1.39%
Air Compressibility Difference		8.60%	Q/Qs	42.95%

Table 31: Energy solution for sample energy analysis case

Radiated	3606.61	Watt
Theoretical	26428.04	Watt
Diffracted	3415.93	Watt
Output	11678.34	Watt
Efficiency	44.19%	-

5.3 Turbine and Air Chamber Effect on the OWC System

The following is a study about how the energy will be transferred into the OWC system: we will study the energy distribution with respect to the turbine constant (both real and imaginary part); and the air chamber volume at calm state (initial air volume

inside the cylinder). We will see how those parameters can affect the energy output from the system. Table 32 is the initial input parameters for the study, and we only change one parameter to see its effect:

Table 32: Input parameters in turbine and air chamber effect study

ω	1	rad/s
h	80	ft
H_{inc}	3	ft
a	8	ft
b	25	ft
V_C	12000	ft^3
Ct-Real	Ct-Imaginary	-
20	0	$(ft^3/s)/(lbf/ft^2)$

First, we study the most important parameter above the water line: the real part of the turbine constant. Usually the real part of the turbine is much larger than the imaginary part of the turbine constant, indicating that the change of air flow is basically in phase with the pressure drop. When we set the imaginary part of the turbine to be zero, the effect of real part of the turbine constant is shown in Table 33:

Table 33: Air flow and energy distribution with real part of turbine constant

Re(Ct)	0	1	12	20	28	40	50
|Pc| (psf)	34	34	31	29	26	23	20
|Qt|(ft^3/s)	0	34	376	577	734	904	1001
P_r (Watt)	4846	4808	4118	3482	2878	2137	1678
P_i (Watt)	26428	26428	26428	26428	26428	26428	26428
P_d (Watt)	3416	3416	3416	3416	3416	3416	3416
P_t (Watt)	8	778	8000	11275	13045	13838	13585
Re(Ct)	90	150	220	280	360	500	600
|Pc| (psf)	13	9	6	5	4	3	2
|Qt| (ft^3/s)	1194	1286	1324	1340	1351	1361	1365
P_r (Watt)	737	308	152	96	59	31	22
P_i (Watt)	26428	26428	26428	26428	26428	26428	26428
P_d (Watt)	3416	3416	3416	3416	3416	3416	3416
P_t (Watt)	10734	7474	5402	4344	3437	2513	2106

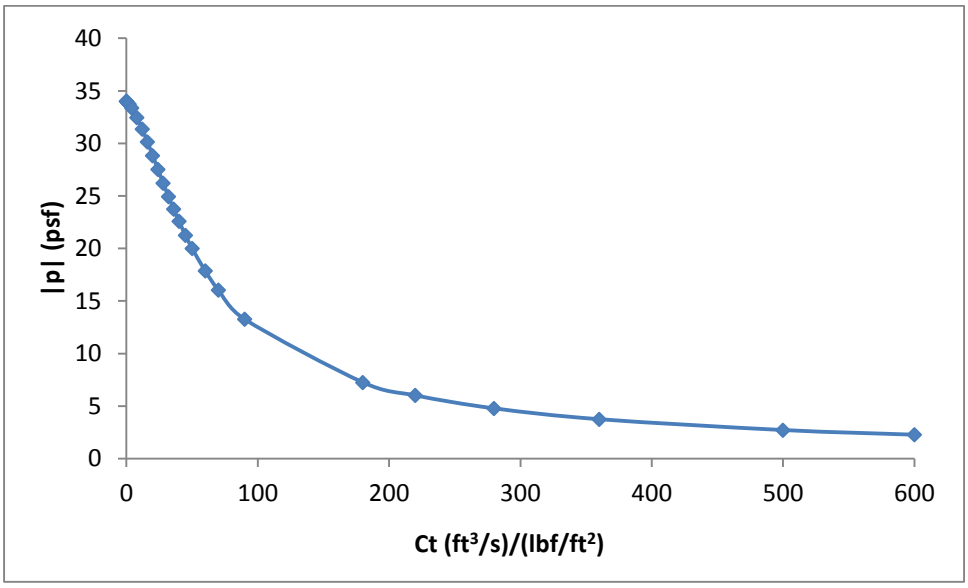

Figure 25. Pressure variation with respect to turbine constant real part

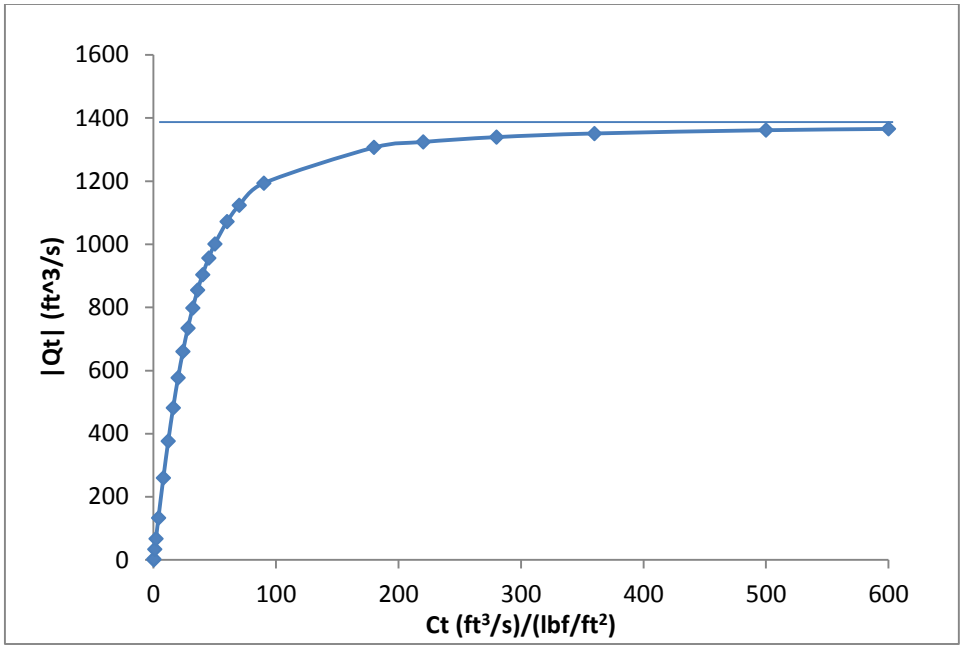

Figure 26. Air flow rate with respect to turbine constant real part

We can find in Figure 25 and 26 that the pressure variation inside the cylinder is decreasing with the increase of the turbine constant; while the air flow inside/outside the cylinder is growing with the increase of the turbine constant, and it converges to the scattering volume flux Q^S, which is reasonable because when the turbine constant goes to infinity, there will not be a turbine at all. $Q^S = 1382.47\ \text{ft}^3/s$ in these cases. Figure 27 shows how the energy is distributed in the system:

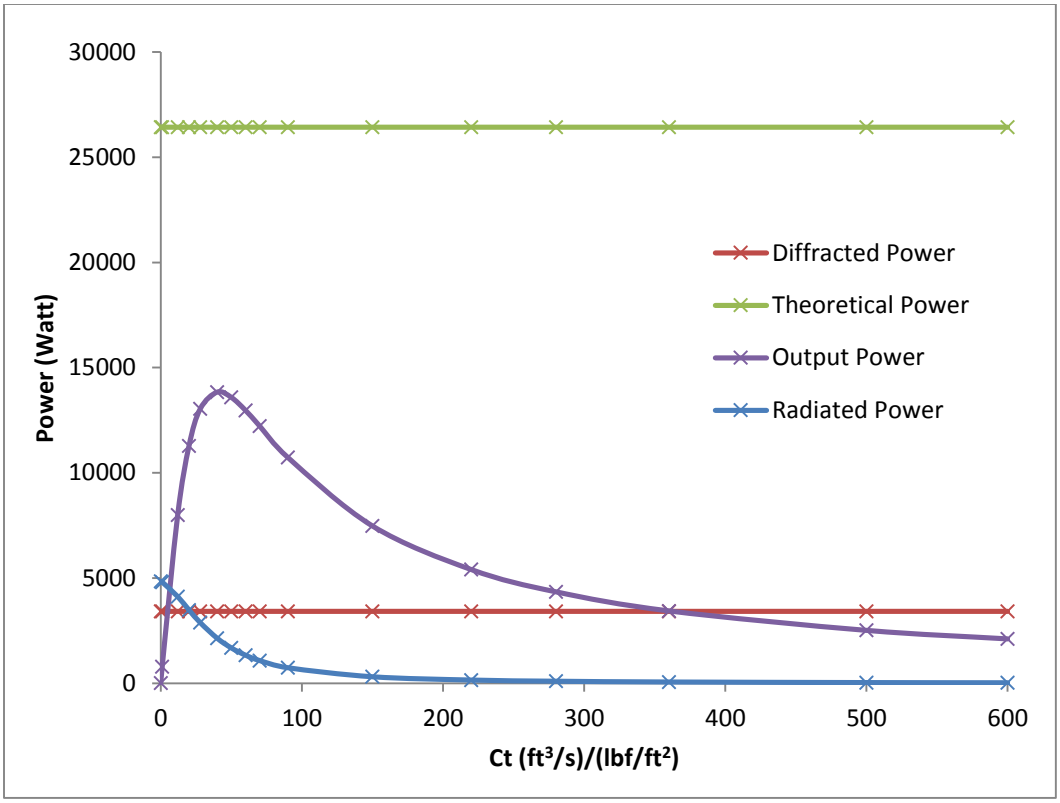

Figure 27. Energy analysis with respect to turbine constant real part

The radiated wave power decays with the turbine constant; the diffracted wave power and theoretical wave power will not change over the turbine constant because they are not related to the air pressure variation inside the cylinder. It can be noticed that the output from the turbine changes greatly over the turbine constant, which makes the optimal design for the air turbine necessary.

Table 34 and Figure 28 show a study about the air chamber volume effect on the energy solution. Air chamber volume at fixed water plane area will be changed to test for the chamber effect on the energy output. Other parameters will stay the same values as in the previous part.

Table 34: Air flow and energy distribution with respect to air chamber volume

V_C	10000	12000	14000	16000	18000	20000
|Pc| (psf)	29.18	28.84	28.50	28.17	27.85	27.53
|Qt|(ft^3/s)	583.62	576.76	570.02	563.40	556.90	550.53
P_r (Watt)	3565.54	3482.13	3401.20	3322.70	3246.54	3172.64
P_t (Watt)	11545.36	11275.25	11013.22	10759.03	10512.41	10273.13
dV/V_C	5.92%	4.90%	4.18%	3.65%	3.23%	2.91%

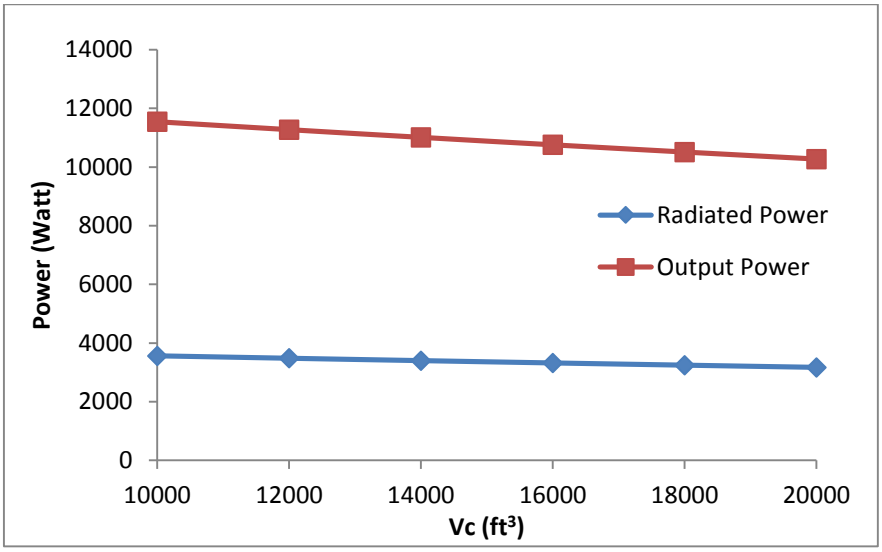

Figure 28. Energy analysis with respect to air chamber volume

We can find that as the chamber volume increases, the magnitude of the pressure variation and air flow both decrease. Theoretical power and diffracted power will not change over the chamber volume. Though the radiated power decreases with respect to the chamber volume, the output is also decreasing with chamber volume at fixed water plane area (fix all the other parameters). However, our model is based on the linearity assumption that the fluctuating air chamber volume V_e is small compared with the

original air chamber volume V_C. So in the computer program OWC Solution, we need to discard the solutions with $dV/V_C>5\%$ because they violate the linear assumption. A nonlinear model is needed to solve for those situations. For now, we need to make the air chamber volume large enough for the cases we calculate. How to calculate the energy output under nonlinear conditions (large volume change) will be a topic for future study.

A study about the effect of imaginary part of the turbine constant to the energy output is shown below. We will change the imaginary part of the turbine constant to test its effect as shown in Table 35 and Figure 29.

Table 35: Energy distribution with imaginary part of turbine constant (Case 1)

Im(Ct)	0	0.4	0.8	1.5
|Pc|(psf)	28.84	29.04	29.25	29.61
|Qt|(ft^3/s)	576.76	580.93	585.38	593.85
P_r (Watt)	3482.13	3531.25	3581.26	3670.99
P_t (Watt)	11275.25	11434.31	11596.26	11886.80
Im(Ct)	2	3	4	6
|Pc|(psf)	29.87	30.41	30.97	32.12
|Qt|(ft^3/s)	600.46	615.08	631.63	670.73
P_r (Watt)	3736.83	3873.06	4015.56	4320.47
P_t (Watt)	12100.00	12541.11	13002.53	13989.85

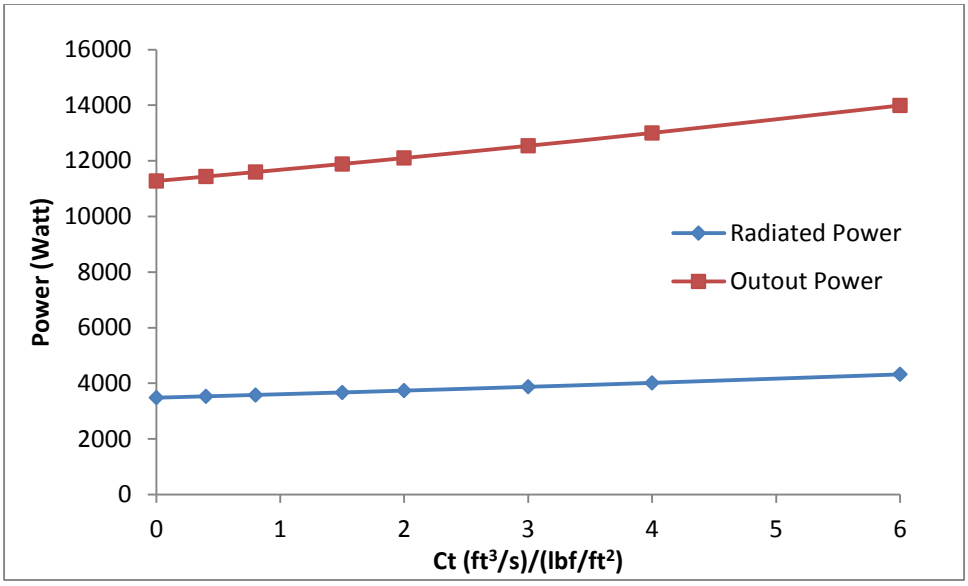

Figure 29. Energy analysis with imaginary part of turbine constant (Case 1)

We can find that the magnitude of pressure drop and air flow will increase with respect to the imaginary part of the turbine constant in this case. The radiated wave power and output power will also increase with respect to the imaginary part of the turbine constant.

However, the imaginary part of turbine constant doesn't necessarily promote the energy output. If we change the incident wave frequency to ω=1.2 rad/s; run the program varying the imaginary part of turbine constant, we can get the results shown in Table 36:

Table 36: Energy distribution with imaginary part of turbine constant (Case 2)

Im(Ct)	0	0.5	1	2
|Pc| (psf)	13.45	13.35	13.24	13.01
|Qt| (ft^3/s)	269.05	267.06	265.14	261.54
Pr (Watt)	60.03	59.11	58.16	56.17
Pt (Watt)	2453.66	2415.92	2376.88	2295.59
Im(Ct)	3	4	5	6
|Pc|(psf)	12.77	12.52	12.26	12.00
|Qt|(ft^3/s)	258.27	255.34	252.74	250.48
Pr (Watt)	54.10	51.99	49.86	47.74
Pt (Watt)	2211.16	2124.87	2037.84	1951.03

We will find that the magnitude of pressure drop and air flow will decrease with respect to the imaginary part of the turbine constant in these cases. Figure 30 shows that the radiated wave power and output power will also decrease with respect to the imaginary part of the turbine constant.

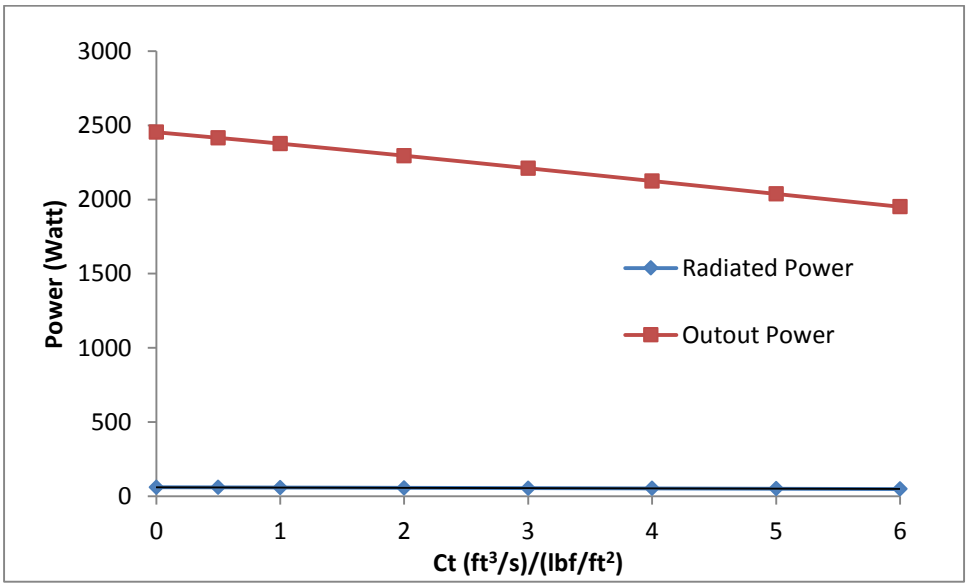

Figure 30. Energy analysis with imaginary part of turbine constant (Case 2)

So the imaginary part of the turbine constant has different effect on the OWC energy output at different frequencies. A detailed study about the turbine constant is done in the next section. Optimization of the complex turbine constant will be the topic that we discuss in the next section.

6. OPTIMIZATION OF THE OWC SYSTEM

6.1 Concept of Optimization

In the previous section, we have developed a method to solve for given wave parameters (frequency, wave height and water depth) and given OWC parameters (radius, draft, chamber volume, turbine constant with possible phase lag). We can attribute the parameters into three categories:

1. Wave parameters: the wave frequency, the wave height and the water depth;

2. “Lower” parameters: the radius, the draft, which are under the water line at calm state;

3. “Upper” parameters: chamber volume, turbine constant including imaginary part, which are above the water line at calm state.

The following part is the optimization for the OWC “Upper” parameters (parameters that are not related to the hydrodynamic problem). The program OWC Solution can automatically optimize the “Upper” parameters, while wave parameters and the “Lower” parameters are set by the researchers.

In the real case, the user of the program OWC Solution can first set the incident wave frequency as the design frequency to the system, then use the equation $\omega_n = \sqrt{\frac{g}{b+0.5a}}$ to evaluate the suitable radius a and draft b for the OWC system.

6.2 Limitations on the Optimization

The optimization for the OWC system is not a purely mathematical problem, we need to set limitations on the variables in the optimization to make the results physically

reasonable. In the optimization process, sometimes you will come across unrealistic solution, which makes the following rules necessary for the optimization:

(1) Conservative motion: The air flow is induced by the fluid free surface volume flux, so it must not have a magnitude larger than the original fluid volume flux. Similarly, the radiated volume flux and air-compressed volume change rate should not have a larger magnitude than the original free surface volume flux. This is a very important condition that must be satisfied.

(2) Turbine constant magnitude: The turbine constant is what we need to select the right turbine. Basically, the turbine constant is a coefficient that determines the ratio of the flow rate to the pressure drop. Experiments have shown a fixed value for turbine constant can be assumed for a given turbine. The magnitude of the turbine constant can theoretically go from 0 to infinity; however, in practice the magnitude should have a range.

The following is why magnitude of turbine constant $|Ct| \epsilon\ (0, \infty)$ theoretically. When the cylinder is completely open at the top, the air inside the cylinder can go freely from the cylinder into the atmosphere. Then, the air flow rate should be very close to the scattering induced volume flux, because the air pressure variation in the cylinder is close to zero (since the air chamber is fully connected to the atmosphere), in equation (5.13) we derived previously:

$$q^S - \frac{i\omega p}{\rho g} q^R = C_t \cdot p_e + \frac{V_C}{k p_a} \cdot p_e \cdot (-i\omega)$$

The radiation terms $\frac{i\omega}{\rho g} q^R$ is a finite value, the air compressibility term $\frac{V_C}{k p_a} \cdot (-i\omega)$ is also finite, so when $p_e \to 0$, they are all 0.

$$q^S = C_t \cdot p_e, \quad p_e \to 0$$

In this case the turbine constant must be ∞.

When the cylinder is completely sealed at the top, the air inside the cylinder cannot flee from the cylinder. The air flow rate through the turbine is zero, but scattering induced volume flux is still there. So the air pressure variation inside the cylinder is not zero. Remind the air water interaction equation (5.13):

$$q^S - \frac{i\omega p}{\rho g} q^R = \frac{V_C}{k p_a} \cdot p_e \cdot (-i\omega), \qquad C_t \cdot p_e = 0$$

So we can tell that $p_e \neq 0$. In this case, the turbine constant must be zero. When the turbine has so much impedance to the air flow, any pressure difference between two sides of the turbine cannot drive the turbine to let go an air flow.

In reality, the turbine constant magnitude is more limited by manufacturing and should be constrained to a smaller range. The computer program OWC Solution has the capability of setting the range of turbine constant magnitudes and optimizing the turbine in the given range. However, as a theoretical exploration to the OWC energy output, we do not apply a more realistic limitation to the turbine constant magnitude.

(3) Turbine Constant imaginary part: The imaginary part of turbine constant will lead to a phase lag, which means the peak of flow rate occurs at a different phase from the pressure variation peak, and this is not negligible for large scale turbines. However, to what extent the phase lag can be created from the turbine is a very

important issue for optimization. In practice, usually I make a 10% limitation to the imaginary part of the constant relative to the real part.

A study about the effect of the limitation to the imaginary part of turbine constant is done below. Set the radius a=4 ft; the draft b=10 ft; the water depth h= 60 ft; the incident wave frequency ω=1.5 rad/s; the incident wave height H_{inc}=2 ft; the air chamber volume V_C=2000 ft^3.

When a 10% limitation is set to the imaginary part of turbine constant, the energy solution is shown in Table 37:

Table 37: Sample optimal solution with a 10% imaginary part limitation

Ct	Real	Imaginary
$(ft^3/s)/(lbf/ft^2)$	8.9188	0.8913
Radiated	191.78	Watt
Theoretical	3735.46	Watt
Diffracted	220.21	Watt
Output	1575.01	Watt
Efficiency	42.16%	
H_{OWC}/H_{inc}	2.236	

The imaginary part of turbine constant is limited to 10% of the real part; a maximum 5.71° phase lag of the turbine is allowed. The system has a medium efficiency.

If we assume no phase lag (zero imaginary part for the turbine constant), the energy solution is shown in Table 38:

Table 38: Sample optimal solution with zero imaginary part limitation

Ct	Real	Imaginary
$(ft^3/s)/(lbf/ft^2)$	8.9615	0.0000
Radiated	174.77	Watt
Theoretical	3735.46	Watt
Diffracted	220.21	Watt
Output	1442.23	Watt
Efficiency	38.61%	
H_{OWC}/H_{inc}	2.236	

The real turbine constant has a mathematical optimal value given by Cho (2002):

$$C_t = \sqrt{\left[Re\left(\frac{\omega}{\rho g}Q^R\right)\right]^2 + [Im(\frac{\omega}{\rho g}Q^R) + \frac{V_C\omega}{kp_a}]^2}$$

The mathematical optimal value is 8.9615 $(ft^3/s)/(lbf/ft^2)$, which perfectly matches the program. The system has a minimum efficiency in this case.

If we assume free turbine constant (Turbine constant is a free complex variable, no limitation to the imaginary part of the turbine constant is applied), the energy solution is shown in Table 39:

Table 39: Sample optimal solution with no imaginary part limitation

Ct	Re	Im
$(ft^3/s)/(lbf/ft^2)$	5.0872	3.8642
Radiated	496.25	Watt
Theoretical	3735.46	Watt
Diffracted	220.21	Watt
Output	2324.69	Watt
Efficiency	62.23%	
H_{OWC}/H_{inc}	2.236	

The system reaches a maximum efficiency. However, the phase lag (75.96%, 37.22°) in this case may not be possible for a real turbine.

The study indicates that in many cases, the phase lag the turbine can reach is an important limitation to the optimization. It can be found from the cases above that the phase lag helps to increase the efficiency of the system, however, the real turbine constant is usually close to a real value with a small imaginary part. According to Falnes (2002), the imaginary part of the turbine constant can be important for a large scale OWC, but it is usually negligible in small scale OWC (usually in laboratory). The computer program OWC Solution has an access to set limitation to the phase lag. Future data about the turbine constant for a real turbine can be applied to get a more realistic result.

(4) Small Volume/Pressure change assumption: This is to ensure the linearity assumption of the system that we made is applied to the cases we are calculating. It will prevent extreme cases in the optimization. In this case, the limitation to the volume/pressure change is set to be 5%. As we have discussed in the previous chapter, nonlinear volume/pressure change OWC system may have better energy output, which can be a future direction that we will be working on.

(5) Minimum Chamber Volume: The minimum chamber volume will prevent the water from flooding the whole chamber, which also ensures the small Volume/Pressure change assumption. This rule is straightforward and unacceptable cases that violate this rule will violate the small volume/pressure change assumption first.

(6) Energy relationship: This is an important limitation to our solutions. The incident wave energy is distributed into many parts, so the following relation is set as a limitation to the solution we get.

The energy input into this system is provided by the incident wave. The energy input rate should be:

$$P_i = \left(\frac{1}{8}\rho g {H_{inc}}^2\right)\frac{\omega}{k}\left[\frac{1}{2}\left(1+\frac{2kh}{sinh(2kh)}\right)\right]\cdot(2a)$$

The air flow power driving the turbine is:

$$P_t = \frac{1}{T}\int_0^T p_e \frac{dV_t}{dt}dt$$

T is the period of the incident wave. The radiated power is:

$$P_r = \frac{1}{T}\int_0^T p_e \frac{iwp}{\rho g}q^R dt$$

Air compressibility doesn't do work through a time period. The diffracted wave power is measured according to the diffracted wave potential:

$$P_d = \frac{1}{8}\rho g \frac{\omega}{k}\left[\frac{1}{2}\left(1+\frac{2kh}{\sinh(2kh)}\right)\right]\int_0^{2\pi} H_d(r,\theta)^2 \cdot r d\theta$$

Koo and Kim (2010) investigated the energy conservation for a 2-D OWC system with viscous loss; for the 3-D OWC system, a conservative limitation is made to the energy balance:

$$P_i \geq P_d + P_r + P_t$$

We will omit the cases that break the energy conservation (with incident frequency very close to the natural frequency). This is especially useful at the natural frequency, because the program gives very large values for the diffracted wave power at

the natural frequency. The energy relationship can help you decide whether you need to reject the solution at frequencies to close to the natural frequency.

When we set the radius a=4 ft; the draft b=10 ft; the water depth h= 60 ft; the incident wave frequency ω=1.6 rad/s; the incident wave height H_{inc}=2 ft; the air chamber volume V_C=2000 ft^3. You will find: H_{OWC}/H_{inc} is 7.452; theoretical power input is 3494.59 Watt; diffracted power is 5087.55 Watt.

That means the solution given by OWC solution should be rejected because it is too close to the natural frequency (ω_n=1.637 rad/s in this case). We base the model on the linear potential theory, when sometimes the assumption we made is violated, the result given by the program should not be applied.

Similar cases occur when we optimize at frequencies too close to the natural frequency. Set the radius a=4 ft; the draft b=10 ft; the water depth h= 60 ft; the incident wave frequency ω=1.573 rad/s; the incident wave height H_{inc}=2 ft; the air chamber volume V_C =2000 ft^3. The energy solution is shown in Table 40:

Table 40: Sample optimal solution limited by the energy relationship

Ct	Real	Imaginary
$(ft^3/s)/(lbf/ft^2)$	0.8097	0.0000
Radiated	1912.78	Watt
Theoretical	3555.98	Watt
Diffracted	1371.99	Watt
Output	271.21	Watt
Efficiency	7.63%	
H_{OWC}/H_{inc}	5.580	

You will find the efficiency for the case is very low. Because near the natural frequency, the diffracted and radiated wave amplitude reaches high values so it tends to violate the energy relationship. Table 41 is the result if we ignore the energy relationship for optimization:

Table 41: A non-physical solution without energy relationship

Ct	Real	Imaginary
$(ft^3/s)/(lbf/ft^2)$	8.0514	0.8000
Radiated	1473.26	Watt
Theoretical	3555.98	Watt
Diffracted	1371.99	Watt
Output	2077.22	Watt
Balance	**-1366.49**	Watt
Efficiency	58.41%	
H_{OWC}/H_{inc}	5.580	

It seems to have a high frequency but you will find the energy have -1366.49 Watt deficit which violates the energy relationship. Table 42 shows the energy solution when we decrease the frequency slightly to ω= 1.55 rad/s:

Table 42: A realistic solution with energy relationship near natural frequency

Ct	Re	Im
$(ft^3/s)/(lbf/ft^2)$	8.3529	0.8341
Radiated	689.63	Watt
Theoretical	3610.28	Watt
Diffracted	642.49	Watt
Output	1974.74	Watt
Efficiency	54.70%	
H_{OWC}/H_{inc}	4.138	

So near the natural frequency, we should be careful about the result given by the program so that the solution we find satisfies all assumption we made.

6.3 The VBA Program for the Optimization

A multi-parameter solver is required for the optimization, which is embedded in my program. Figure 31 is the input/output screen of the VBA program named OWC Solution. In my research, almost all the calculations are conducted in the program, while the Excel worksheet serves as a convenient input and output tool for us. You can calculate for given OWC and wave parameters by clicking on "SOLVE"; or find the optimal solution by clicking "OPTIMIZE".

	A	B	C	D	E	F	G	H	I	J	K	L
1	ω	1	rad/s	a	10	ft	Vc	8000	ft^3			
2	h	60	ft	b	20	ft	Re	Im				
3	Hinc	2	ft	γ	1.4	Ct	19.242	1.917	(ft^3/s)/(lbf/ft^2)			
4	r	0	ft									
5	θ	0	rad	SOLVE		OPTIMIZE						
6	γ	0	ft									
7	Hydrodynamic Solution									Total Vlomue Flux		
8	k	0.032	k1	0.042	k2	0.100	k3	0.154		Re	Im	Mag
9	Howc	3.470	0.192	3.475	λ	194.02	No	1.9060		-290.081	265.569	393.286
10	Cp	17.904	Howc/Hinc	1.738	T	6.283	Howc/λ	0.0179		Air Compressibility Volume Flux		
11	VolFLuxS	-36.74	665.37	666.38	ft^3/s					Re	Im	Mag
12	VolFLuxR	-1469.42	-200.80	1483.07	ft^3/s					-35.550	-42.154	55.144
13	Linear Solution									Radiated Volume Flux		
14	Pc	Re	Im	|Pc|	θp	0.965%	essue change			Re	Im	Mag
15	psf	-15.611	13.166	20.431	139.834	978.232	Pa			-253.337	-399.801	473.308
16	Qt	Re	Im	|Qt|	θq	11.189	m^3/s			Qs(power)	6327.37	Watt
17	ft^3/s	-325.631	223.414	394.905	145.581	5445.044	Watt			Radiated	887.18	Watt
18		Re	Im	Magnitude	Efficiency	35.04%				Theoretical	15538.34	Watt
19	Incident	0.808	0.589	1.000	Diffraction	Test Point	Power			Diffracted	692.18	Watt
20	Diffraction	-0.261	0.719	0.765	0.435	3	692.18			Output	5445.04	Watt
21	-	Re	Im	Magnitude	Radiation	Test Point	Power			Transmitted	8518.79	Watt
22	Ar	0.286	-5.180	5.188	0.382	5	888.26					
23	Qt Difference		59.26%	dV/Vc	4.92%							
24	Radiation Difference		71.03%	dp/Pa	0.97%							
25	AirCompr Difference		8.28%	Q/Qs	59.02%							

Figure 31. OWC Solution Program

Yellow cells contain input parameters; purple cells are input parameters that can be changed for optimization, and they acts like yellow cells when you just solve for given parameters by clicking "SOLVE". Orange cells represent variables; blue cells are calculation results for the solved variables; green cells are the cylindrical coordinates for more extensive calculations that can be done with the program. Usually, they are all set to be zero; but you can also calculate the response at other coordinates by setting the right value in the green cells. White cells are units for the variables.

6.4 Results of Optimization

Table 43, 44, 45, and 46 consist a complete optimization case:

Table 43: Input parameters for optimization (Case 1)

ω	1.75	rad/s
h	30	ft
H_{inc}	2	ft
a	4	ft
b	10	ft
γ	1.4	-
V_C	2000	ft^3
Ct-Real	Ct-Imaginary	-
7.542	0	$(ft^3/s)/(lbf/ft^2)$

Table 44: Hydrodynamic solution for optimization (Case 1)

k	0.096	k_1	0.074
k_2	0.194	k_3	0.304
Cp	9.469	T	3.590
λ	65.590	**H_{OWC}/H_{inc}**	**1.899**
-	Real	Imaginary	Magnitude
$VolumeFLux^S$	-38.968	-162.421	167.030
$VolumeFLux^R$	-60.693	112.056	127.437

Table 45: Air flow and motion analysis results for optimization (Case 1)

Pc	Real	Imaginary	|Pc|	θp(°)
(psf)	-11.876	-8.538	14.626	-144.288
Qt	Real	Imaginary	|Qt|	θq(°)
(ft^3/s)	-89.574	-64.394	110.319	-144.288
Qt Difference		66.05%	dV/Vc	3.19%
Radiation Difference		76.30%	dp/Pa	0.69%
Air Compressibility Difference		10.34%	Q/Qs	66.85%

Table 46: Energy solution for the optimization (Case 1)

Radiated	159.92	Watt
Theoretical	26428.04	Watt
Diffracted	3415.93	Watt
Output	11678.34	Watt
Efficiency	33.28%	-

Table 47, 48, 49, and 50 consist a complete solution when we change the incident wave frequency:

Table 47: Input parameters for optimization (Case 2)

ω	1.55	rad/s
h	30	ft
H_{inc}	2	ft
a	4	ft
b	10	ft
V_C	2000	ft^3
Ct-Real	Ct-Imaginary	-
7.785	0.777	$(ft^3/s)/(lbf/ft^2)$

Table 48: Hydrodynamic solution for optimization (Case 2)

k	0.076	k_1	0.080
k_2	0.197	k_3	0.306
Cp	11.126	T	4.054
λ	82.425	**H_{OWC}/H_{inc}**	**4.272**
-	Real	Imaginary	Magnitude
$VolumeFLux^S$	-51.355	328.870	332.856
$VolumeFLux^R$	-77.748	-246.588	258.554

Table 49: Air flow and motion analysis results for optimization (Case 2)

Pc	Real	Imaginary	|Pc|	θp(°)
(psf)	-16.929	9.983	19.653	149.473
Qt	Real	Imaginary	|Qt|	θq(°)
(ft^3/s)	-139.548	64.569	153.762	155.170
Qt Difference		46.19%	dV/Vc	4.94%
Radiation Difference		77.68%	dp/Pa	0.93%
Air Compressibility Difference		6.18%	Q/Qs	45.99%

Table 50: Energy solution for the optimization (Case 2)

Radiated	776.47	Watt
Theoretical	3862.52	Watt
Diffracted	718.42	Watt
Output	2038.43	Watt
Efficiency	52.77%	-

Table 51, 52, 53, and 54 consist the complete solution when we change the incident wave frequency to 1.35 rad/s:

Table 51: Input parameters for optimization (Case 3)

ω	1.35	rad/s
h	30	ft
H_{inc}	2	ft
a	4	ft
b	10	ft
V_C	2000	ft^3
Ct-Real	Ct-Imaginary	-
4.341	0.434	$(ft^3/s)/(lbf/ft^2)$

Table 52: Hydrodynamic solution for optimization (Case 3)

k	0.060	k_1	0.085
k_2	0.200	k_3	0.308
Cp	13.511	T	4.654
λ	104.97	**H_{OWC}/H_{inc}**	**1.643**
-	Real	Imaginary	Magnitude
$VolomeFLux^S$	-1.814	111.489	111.504
$VolumeFLux^R$	-45.094	-45.486	64.051

Table 53: Air flow and motion analysis results for optimization (Case 3)

Pc	Real	Imaginary	|Pc|	θp(°)
(psf)	-12.329	13.849	18.543	131.670
Qt	Real	Imaginary	|Qt|	θq(°)
(ft3/s)	-59.529	54.767	80.890	137.391
Qt Difference		72.54%	dV/Vc	3.00%
Radiation Difference		57.44%	dp/Pa	0.88%
Air Compressibility Difference		15.15%	Q/Qs	72.62%

Table 54: Energy solution for the optimization (Case 3)

Radiated	50.15	Watt
Theoretical	4690.36	Watt
Diffracted	58.56	Watt
Output	1011.71	Watt
Efficiency	21.57%	-

The solution shows incident wave frequency has great effect on the energy output from given OWC system.

Table 55 and Figure 32 show a sample optimization in the frequency domain. The radius a=10 ft; the draft b= 20 ft; the water depth h= 60 ft; the incident wave height H_{inc}= 2 ft; chamber volume V_C=8000 ft^3.

Table 55: Optimal solution with respect to frequency (Case 1)

ω (rad/s)	Radiated	Theoretical	Diffracted	Output	Efficiency	H_{OWC}/H_{inc}
0.6	37.5	27040.2	27.4	2669.9	9.87%	1.085
0.8	127.0	20797.3	113.2	3511.5	16.88%	1.255
1	850.8	15538.3	692.2	5514.3	35.49%	2.121
1.07	4538.5	14122.6	3399.0	6102.8	43.21%	3.855
1.2	416.9	12085.8	7879.9	3789.0	31.35%	2.288
1.3	172.5	10943.4	4815.0	1808.2	16.52%	0.751
1.5	14.1	9338.7	6052.1	487.0	5.21%	0.198

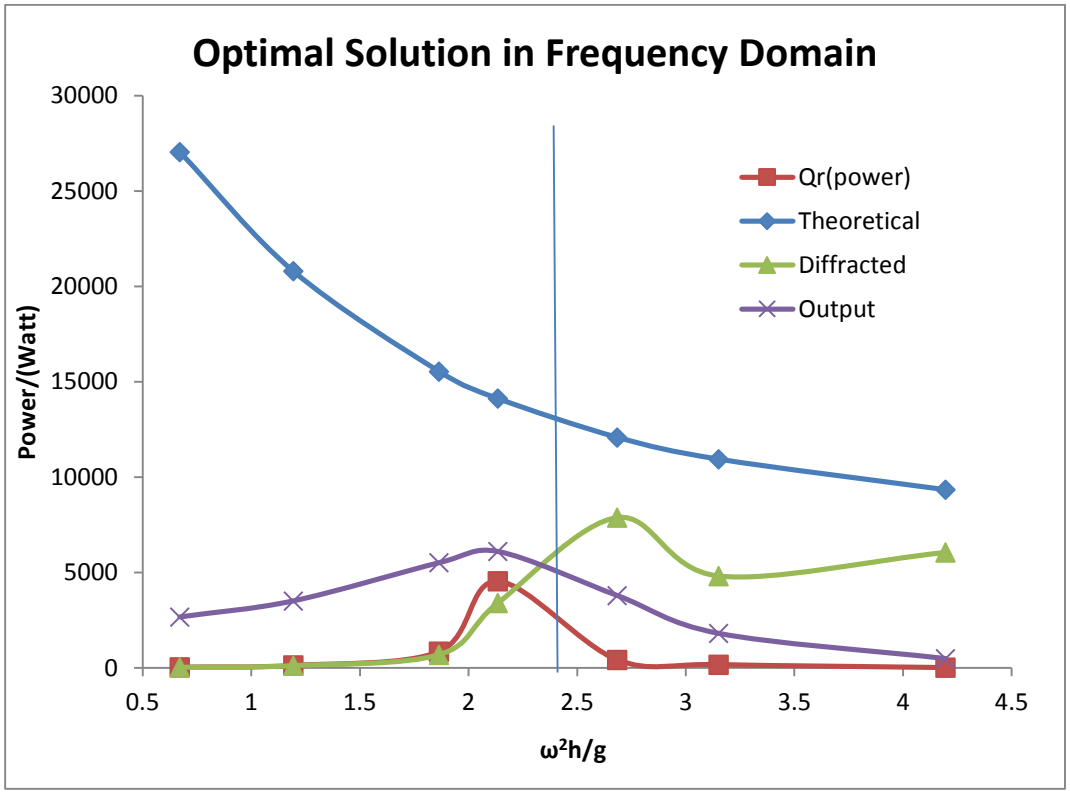

Figure 32. Optimal OWC energy solution with respect to frequency (Case 1)

We can find ω_n =1.134 rad/s; $\omega_n{}^2 h/g = 2.4$. The peak of the maximum energy output does not show at the natural frequency because at the natural frequency the radiated and diffracted power is also large.

Table 56 and Figure 33 show another sample optimization in the frequency domain. The radius a=10 ft; the draft b= 20 ft; the water depth h= 60 ft; the incident wave height H_{inc}= 2 ft; the chamber volume V_C= 12000 ft^3.

Table 56: Optimal solution with respect to frequency (Case 2)

ω	Radiated	Theoretical	Diffracted	Output	Efficiency	H_{OWC}/H_{inc}
0.6	28.9	27040.2	27.4	2349.4	8.69%	1.085
0.8	104.7	20797.3	113.2	3191.6	15.35%	1.255
1	629.1	15538.3	692.2	5424.5	34.91%	2.121
1.07	3071.8	14122.6	3399.0	7651.9	54.18%	3.855
1.2	389.7	12085.8	7879.9	3816.2	31.58%	2.288
1.3	214.9	10943.4	4815.0	2007.1	18.34%	0.751
1.5	14.1	9338.7	6052.1	556.9	5.96%	0.198

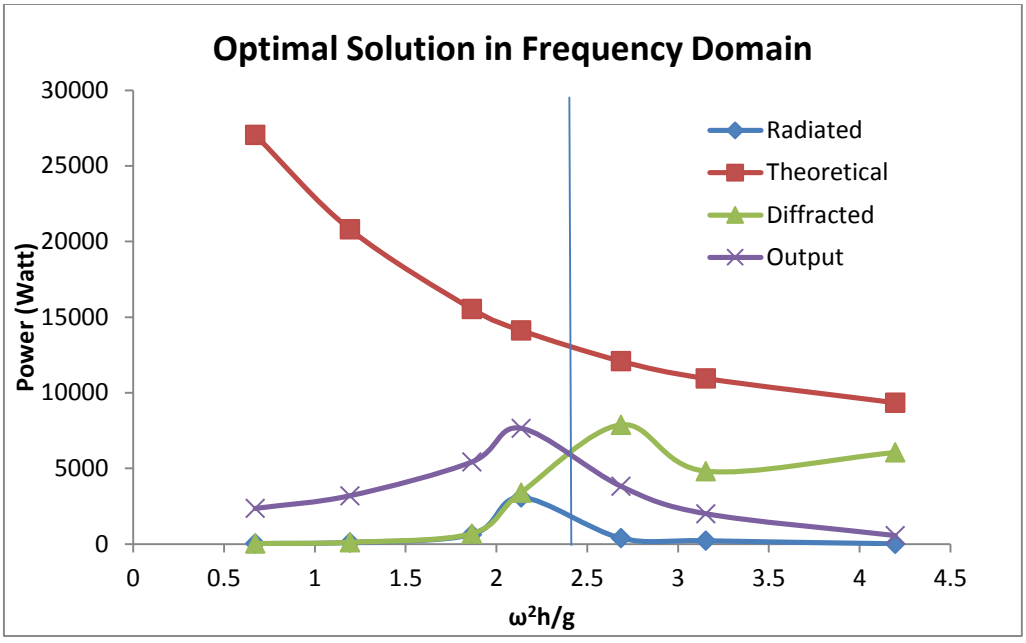

Figure 33. Optimal OWC energy solution with respect to frequency (Case 2)

Still, ω_n =1.134 rad/s; $\omega_n{}^2 h/g = 2.4$. The maximum energy output is improved because we made the linearity assumption of small volume change. However, in practice the volume of the air chamber cannot be too large so it is a balance between efficiency and cost.

6.5 Typical Design Process

The following is an example about the optimization design process. Given the incident wave height H_{inc}=2 ft; the incident wave frequency ω=0.8 rad/s; the water depth h=100 ft; and we want to extract energy from a width of 20 ft, so the radius a=10 ft; air chamber volume is 16000 ft^3.

Base on the design frequency, (b+a/2) should be around 50.26 ft, and b should be around 45.26 ft. A detailed result about different design draft is shown in Table 57:

Table 57: Select the draft for best efficiency

b (ft)	40	41	42	47	48	49	50
Radiated	1236	2219	4495	4554	1891	890	507
Theoretical	19166	19166	19166	19166	19166	19166	19166
Diffracted	1265	2113	4190	7415	4204	2836	2123
Output	8576	9300	9758	7196	8919	7914	6627
Efficiency	44.75%	48.53%	50.91%	37.55%	46.54%	41.29%	34.58%
RAO	3.384	4.194	5.614	5.233	3.625	2.735	2.172

It can be noticed that there is a jump from 42 ft to 47 ft. When the draft makes the design frequency too close to the incident wave frequency, the radiated and diffracted wave power will reach peak value, which lowers the output power or breaks the linearity assumption we made. So the best design draft b=42 ft. The optimal turbine constant is: 28.45+2.84i (ft^3/s) /(lbf/ft^2).This is a complete OWC system with output efficiency 50.91%.

6.6 Discussion about the Turbine

We can observe from the cases in the previous sections that the computer program OWC Solution is able to determine the optimal turbine constant for each case. In this subsection, the author will discuss the availability of the turbine with our desired turbine constant. Wells turbine is usually used in OWC system to extract the wave energy. Gato and Falcão (1984, 1988) have studied the aerodynamics of the Wells turbine using numerical model, however, it is easier to find the performance of a Wells turbine in a given OWC system if we have the experiment data of a Wells turbine.

Scholars such as Kaneko, Setoguchi and Inoue (1986) and Camporeale, Filianoti and Torresi (2011) have provided the experiment performance data of Wells turbine.

As an example, consider the case of the cylinder tested in the UNO towing tank by Garriga and Falzarano (2008). The radius of the cylinder is 1 ft; the draft of the cylinder is 2.5ft; the water depth is 6.33 ft; the incident wave height is 1 ft; the incident wave frequency is 3 rad/s and the volume of air chamber is 70 ft^3. This is a small scale case that will be used as an illustration for the selection of air turbine.

Since this is a small scale case, the imaginary part of the turbine constant is negligible. The computer program OWC Solution gives the following solution of the maximum energy input to the turbine: turbine constant is 1.061 $(ft^3/s)/(lbf/ft^2)$; H_{OWC}/H_{inc} is 2.298; pressure variation is 8.621 psf; air flow magnitude through the turbine is 9.151 ft^3/s; output energy is 53.48 Watt with 40.87% transfer efficiency from the incident wave power.

This design can be realized with a small scale Wells turbine already built and tested by Camporeale, Filianoti and Torresi (2011). They used the following nondimensional values in their experiments on the Wells turbine performance in oscillating flow:

$$p' = \frac{p}{\rho_a {\omega_t}^2 {R_{tip}}^2}$$

$$v' = \frac{Q_t}{\pi({R_{tip}}^2 - {R_{hub}}^2)\omega_t R_{tip}}$$

In which p' and v' is the pressure drop and average axial velocity in nondimensional form, ρ_a is the density of air at 0°C, ω_t is the angular rotation speed of the turbine. Camporeale, Filianoti and Torresi's (2011) experiments have given the pressure drop (p') curve versus average axial velocity (v') for a Wells turbine with hub radius R_{hub}=101mm=0.331 ft, tip radius R_{tip}= 155mm=0.5 ft, blade chord 74 mm, 7 blades ,constant chord and NACA0015 blade profile.

Rotational speed ω_t can be changed to adjust the turbine constant of this existing turbine to meet our design as shown in Table 58:

Table 58: Select the rotational speed for the turbine

N (rpm)	ω_t (rad/s)
1284.84	134.55
v'	p'
0.3	0.75

When the average axial velocity v'=0.3; pressure drop p'=0.75 according to Camporeale, Filianoti and Torresi's (2011) experiments. So when we dimensionalize the pressure drop and air flow rate, the pressure drop is 8.621 psf; the air flow magnitude through the turbine is 9.151 ft^3/s, which agrees with the real turbine constant 1.061 $(ft^3/s)/(lbf/ft^2)$ that we determined in the design/optimization process. The rotational speed of 1284.84 rpm is a reasonable rotational speed for the Wells turbine that Camporeale, Filianoti and Torresi (2011) have tested.

It can be found from the case above that the existing air turbine can be used to realize our design for the OWC system if we have the experimental data of pressure drop versus axial air flow velocity, which is a typical test for an air turbine.

The optimal value for the air turbine constant can be used to design new air turbines as well as to select from existing air turbines with their performance data.

In the following case, the radius of the cylinder is 5 ft; the draft of the cylinder is 10 ft; the water depth is 60 ft; the incident wave height is 2 ft; the incident wave frequency is 1.5 rad/s and the volume of air chamber is 3500 ft^3.

My computer program OWC Solution gives the following solution of the maximum energy input to the turbine: turbine constant is 17.44+1.74i $(ft^3/s)/(lbf/ft^2)$; H_{OWC}/H_{inc} is 2.692; output energy is 2605.94 Watt with 55.81% transfer efficiency from the incident wave power. We will choose an air turbine from the six turbines below in Table 59:

Table 59: Select the right turbine

Re(Ct)	Im(Ct)	Efficiency
16	0	51.41%
18	0	51.57%
20	0	51.22%
16	1.5	55.36%
17	1	54.03%
20	1	53.27%

OWC Solution can find the turbine with the highest efficiency at certain frequency: we will choose the turbine with complex turbine constant 16+1.5i $(ft^3/s)/(lbf/ft^2)$.

Through the discussion above, we need to have knowledge about the curve of pressure drop versus the air flow rate to decide the right turbine for our design.

7. CONCLUSION

The numerical results on the free surface elevation inside the cylinder agree reasonably well with the experimental results given by Garriga and Falzarano (2008) obtained in the UNO towing tank. The ratio between the wave height at the center of cylinder and the incident wave height has a typical transfer function shape with obviously different values only at a small frequency range near the natural frequency.

The geometric parameters of the cylinder (radius and draft) determine the natural frequency and the wave height transfer function, in which draft has a more significant effect. Water depth will also influence the fluid field with bottom effect obvious when draft comes close to water depth. Wave radiation from the OWC system also shows a similar transfer function with peak values at the same natural frequency decided by geometric parameters.

The extended study on the energy output from the OWC system indicates that there exists an optimal design for the air turbine to extract energy from the incident waves. And the highest efficiency from the system can be found near the natural frequency. The possible phase lag (between air flow and pressure drop) that an air turbine can reach is very important to the OWC efficiency.

8. FUTURE WORK

Further research can be done on:

1. Calculate the numerical results using other numerical model such as WAMIT and make a comparison with given results.

2. Undertake a research on the turbine aerodynamics, model for the air turbine to calculate the torque and power directly output from the turbine.

3. Explore the solution to the OWC system with nonlinearity in the motion of air flow and air compressibility.

4. Verify the numerical results with more experiments for the truncated vertical cylinder, including open top cylinder and turbine connected cylinder.

5. Modify the numerical model with viscous effect to have better approximation to real situations.

6. Model the generator connected to the air turbine to calculate the electricity output from the OWC system.

REFERENCES

Abramowizt, M. A. and Stegun, I., 1964. Handbook of Mathematical Functions. Dover Publications, New York, NY.

Alves, M., Vicente, M., , A. J. N. A. and Guerinel, M., 2011. Implementation and Verification of a Time Domain Model to Simulate the Dynamics of OWCs. 9th European Wave and Tidal Energy Conference. Southampton, UK. Retrieved from: http://www.see.ed.ac.uk/ ~shs/EWTEC% 202011%20full/papers/246.pdf.

Camporeale, S. M., Filianoti, P. and Torresi M., 2011. Performance of a Wells turbine in an OWC Device in Comparison to Laboratory Tests. 9th European Wave and Tidal Energy Conference. Southampton, UK. Retrieved from: http://www.see.ed.ac.uk/~shs/EWTEC%202011%20full/papers/244.pdf.

Chakrabarti, S. K., 1987. Hydrodynamics of Offshore Structures. WIT Press, Southampton, UK.

Cho, I.H., 2002. Wave Energy Absorption by a Circular Oscillating Water Column Device. Journal of Korean Society of Coastal and Ocean Engineers. Vol. 14(1), pp. 8-18.

Dean, R. G. and Dalrymple, R. A., 1984. Water Wave Mechanics for Engineers and Scientists. World Scientific Publishing, Singapore.

Evans, D. V., 1982. Wave-power Absorption by Systems of Oscillating Surface Pressure Distributions. Journal of Fluid Mechanics. Vol. 114, pp. 481-499.

Evans, D. V. and Porter, R., 1995. Hydrodynamic Characteristics of an Oscillating Water Column Device. Applied Ocean Research. Vol. 17, pp. 155-164.

Evans, D. V. and Porter, R., 1997. Efficient Calculation of Hydrodynamic Properties of OWC-Type Devices. Journal of Offshore Mechanics and Arctic Engineering. Vol. 119, pp. 210-218.

Falnes, F., 2002. Ocean Waves and Oscillating Systems. Cambridge University Press, Cambridge, UK.

Faltinsen, O. M., 1990. Sea Loads on Ships and Offshore Structures. Cambridge University Press, Cambridge, UK.

Falzarano, J. M. et al., 2012. Offshore Renewable Energy. Proceedings of the 18th International Ship and Offshore Structures Congress. Rostock, Germany. Vol. 2, pp. 153-200.

Garrett, C. J. R., 1970. Bottomless Harbours. Journal of Fluid Mechanics. Vol. 43, pp. 433-449.

Garriga, O. S. and Falzarano, J. M., 2008. Water Wave Interaction on a Truncated Vertical Cylinder. Journal of Offshore Mechanics and Arctic Engineering. Vol. 130, pp. 031002(1-8).

Garriga, O. S., 2003. Water Waves and Marine Structure Interaction. Master's thesis, University of New Orleans, New Orleans, LA.

Gato, L. M. C. and Falcão, A. F. de O., 1984. On the Theory of the Wells Turbine. Journal of Engineering for Gas Turbines and Power. Vol. 106(3), pp. 628-633.

Gato, L. and Falcão, A. F. de O., 1988. Aerodynamics of the Wells Turbine. International Journal of Mechanical Sciences. Vol. 30(6), pp. 383-395.

Haberman, R., 2004. Applied Partial Differential Equations with Fourier Series and Boundary Value Problems. Pearson Education, Upper Saddle River, NJ.

Kaneko, K., Setoguchi, T. and Inoue, M., 1986. Performance of Wells Turbine in Oscillating Flow. Proceedings of the Current Practices and New Technology in Ocean Engineering. New Orleans, LA. Vol. 2, pp. 447–452.

Karami, V., Ketabdari, M.J. and Akhtari, A. K., 2012. Numerical Modeling of Oscillating Water Column Wave Energy Convertor. International Journal of Advanced Renewable Energy Research. Vol. 1(4), pp. 196-206.

Koo, W. and Kim, M., 2010. Nonlinear Time-Domain Simulation of a Land-Based Oscillating Water Column. Journal of Waterway, Port, Coastal, Ocean Engineering. Vol. 136(5), pp. 276–285.

Koo, W. and Kim, M., 2012. Numerical Analysis of a Fixed-type Oscillating Water Column with Irregular Waves. Proceedings of the Twenty-second (2012) International Offshore and Polar Engineering Conference. Rhodes, Greece. Vol. 1, pp. 576-581.

Linton, C. M. and Evans, D. V., 1992. The Radiation and Scattering of Surface Waves by a Vertical Circular Cylinder in a Channel. Philosophical Transactions of the Royal Society of London. Vol. 338, pp. 325-357.

Malmo, O. and Reitan, A., 1985. Wave-power Absorption by an Oscillating Water Column in a Channel. Journal of Fluid Mechanics. Vol. 158, pp. 153-175.

Sarmento, A. J. N. A. and Falcão, A. F. de O., 1985. Wave Generation by an Oscillating Surface Pressure and Its Application in Wave-energy Extraction. Journal of Fluid Mechanics. Vol. 150, pp. 467-485.